DNA methylation-environment interactions in the human genome

Rachel A. Johnston[1,2,3], Katherine A. Aracena[4], Luis B. Barreiro[4,5,6], Amanda J. Lea[7,8], Jenny Tung[1,8, 9,10,11]

[1]Department of Evolutionary Anthropology, Duke University, Durham, NC 27708, USA
[2]Zoo New England, Boston, MA 02121, USA
[3]Broad Institute of MIT and Harvard, Cambridge, MA 02142, USA
[4]Department of Human Genetics, University of Chicago, Chicago, IL 60637, USA
[5]Section of Genetic Medicine, Department of Medicine, University of Chicago, Chicago, IL 60637, USA
[6]Committee on Immunology, University of Chicago, Chicago, IL 60637, USA
[7]Vanderbilt University, Nashville, TN 37240, USA
[8]Canadian Institute for Advanced Research, Toronto, Canada M5G 1Z8
[9]Duke Population Research Institute, Duke University, Durham, NC 27708, USA
[10]Department of Biology, Duke University, Durham, NC 27708, USA
[11]Department of Primate Behavior and Evolution, Max Planck Institute for Evolutionary Anthropology, 04103 Leipzig, Saxony, Germany

*Corresponding author: E-mail: jtung@eva.mpg.de; racheljohnston7@gmail.com

Abstract

Previously we showed that a massively parallel reporter assay, mSTARR-seq, could be used to simultaneously test for both enhancer-like activity and DNA methylation-dependent enhancer activity for millions of loci in a single experiment (Lea *et al*., 2018). Here we apply mSTARR-seq to query nearly the entire human genome, including almost all CpG sites profiled either on the commonly used Illumina Infinium MethylationEPIC array or via reduced representation bisulfite sequencing. We show that fragments containing these sites are enriched for regulatory capacity, and that methylation-dependent regulatory activity is in turn sensitive to the cellular environment. In particular, regulatory responses to interferon alpha (IFNA) stimulation are strongly attenuated by methyl marks, indicating widespread DNA methylation-environment interactions. In agreement, methylation-dependent responses to IFNA identified via mSTARR-seq predict methylation-dependent transcriptional responses to challenge with influenza virus in human macrophages. Our observations support the idea that pre-existing DNA methylation patterns can influence the response to subsequent environmental exposures—one of the tenets of biological embedding. However, we also find that, on average, sites previously associated with early life adversity are not more likely to functionally influence gene regulation than expected by chance.

Introduction

DNA methylation is sensitive to the environment, can remain stable across cell divisions, and in some contexts, can alter gene regulation. Consequently, it has received a high level of attention as a potential pathway linking environmental exposures to downstream trait variation, especially when these exposures are separated temporally, as proposed by the "biological embedding" hypothesis (Hertzman, 1999; Hertzman, 2012). In a canonical example, gestational manipulation of methyl donors in mice is causally implicated in changes in DNA methylation and expression levels of the *agouti* gene, which in turn affects susceptibility to obesity and insulin resistance later in life (Dolinoy *et al.*, 2006). However, the mechanism underlying the *agouti* case—"metastable" methylation of an inserted intracisternal A particle [IAP] class retrovirus—is now thought to be unusual (Kazachenka *et al.*, 2018). Thus, it remains unclear whether the many reports of environment-DNA methylation associations are likely to represent links along a causal pathway to phenotype, or are better viewed as passive biomarkers of exposure.

Experimental tests of the causal impact of DNA methylation on gene regulation indicate that both scenarios are possible. *In vitro* studies reveal that transcription factor binding is frequently (but not ubiquitously) sensitive to DNA methylation (O'Malley *et al.*, 2016; Yin *et al.*, 2017). More recently, epigenomic editing of DNA methylation marks has been shown to alter the activity of transcription factors important in disease and development *in vivo* (Greenberg and Bourc'his, 2019; Yim *et al.*, 2020), as well as the formation of CTCF-mediated gene loops (Lei *et al.*, 2017). However, other epigenetic editing studies show that, even within the same regulatory element, changes in DNA methylation have functional consequences for gene expression at only a subset of sites (e.g. (Maeder *et al.*, 2013). Indeed, in the native genome, enhancer activity appears to be insensitive to DNA methylation levels in the majority of cases (Kreibich *et al.*, 2023). Time series analyses in human dendritic cells have also shown that, in response to a pathogen challenge, nearly all changes in gene expression precede changes in DNA methylation (Pacis *et al.*, 2019). Such methylation changes may nevertheless be functionally relevant if they influence the speed and magnitude of subsequent challenges (e.g., by marking the accessibility of latent enhancers across cell divisions) (Kamada *et al.*, 2018; Sun and Barreiro, 2020). This hypothesis may explain, for example, enhanced transcriptional responses to glucocorticoid stimulation in the descendants of hippocampal progenitor cells previously challenged with glucocorticoids (Provençal *et al.*, 2020).

Together, these findings suggest that environment-associated DNA methylation marks are mixed sets that include functionally silent sites, sites that are constitutively important for gene regulation, and sites in which DNA methylation levels affect gene regulation only under certain conditions. Disentangling which sites belong to which set is important for interpreting and prioritizing the results of a growing body of studies in the biological, social, and health sciences, especially those that test hypotheses that assume a functional role for DNA methylation, such as biological embedding (Hertzman, 2012; Demetriou *et al.*, 2015; Aristizabal *et al.*, 2020). To facilitate this process, we recently introduced a massively parallel reporter assay, mSTARR-seq, that is capable of testing the functional effects of DNA methylation on regulatory activity in high-throughput (Lea *et al.*, 2018). This method allowed us to test for methylation-dependent regulatory activity at millions of CpG sites in the human genome. However, our previous data set did not investigate how DNA methylation marks affect the response to environmental challenge. It also did not explicitly target the CpG sites that are the

most commonly assayed in the human genome (i.e., those featured on the Illumina MethylationEPIC array).

Here, we address these gaps by using mSTARR-seq to construct a genome-wide map of DNA methylation-dependent enhancer activity for 27.3 million CpG sites in the human genome (93.5% of those in the human genome as a whole). This set includes 99.3% of CpG sites present on the Illumina MethylationEPIC array, the most commonly used platform for profiling DNA methylation in humans, and 99.4% of CpG sites accessible via reduced-representation bisulfite sequencing (RRBS; (Meissner *et al.*, 2005)). To evaluate the importance of DNA methylation in responses to environmental challenge, we performed mSTARR-seq under baseline conditions (i.e., no challenge) and following exposure to two physiologically relevant environmental challenges: dosage with the synthetic glucocorticoid dexamethasone, which plays a central role in metabolic regulation and stress-related homeostasis, and interferon alpha (IFNA), a cytokine that elicits genomic and immunological responses associated with viral infection.

We used these data to pursue three goals. First, we describe overall patterns of regulatory activity and methylation-dependent regulatory activity across profiled sites, including how sites targeted by the EPIC array or by RRBS compare to the genome as a whole. The results of this analysis produce a new resource: a map of DNA methylation-dependent enhancer activity across the human genome. Second, we test the degree to which methylation-dependent regulatory activity is affected by exposure to steroid hormone or immune defense-related signaling molecules. Our results yield insight into the frequency of DNA methylation-environment interactions genome-wide, and provide support for the hypothesis that DNA methylation potentiates the cellular response to external stressors. Finally, we illustrate the applicability of this resource by testing two predictions of the biological embedding hypothesis: that pre-existing DNA methylation levels can affect the transcriptional response to subsequent environmental challenge (Provençal *et al.*, 2020; Sun and Barreiro, 2020; Fanucchi *et al.*, 2021), and that sites linked to early life adversity (ELA) are likely to be functionally important for shaping gene expression. Our results suggest that mSTARR-seq can identify DNA methylation-environment interactions that also occur *in vivo* in human populations and can therefore help prioritize environment and ELA-associated loci for future follow-up.

Results

mSTARR-seq captures enhancer activity and methylation-dependent enhancer activity genome-wide

We assessed regulatory activity and methylation-dependent regulatory activity for 4,558,475 600-base pair windows of the genome by pairing hybridization capture of targeted loci in the human genome with the massively parallel reporter assay, mSTARR-seq (Lea *et al.*, 2018). In brief, mSTARR-seq performs enzymatic manipulation of DNA methylation across hundreds of thousands to millions of reporter DNA fragments simultaneously. By measuring the ability of fragments to self-transcribe (as in (Arnold *et al.*, 2013; Shlyueva *et al.*, 2014); reviewed in (Gallego Romero and Lea, 2022)), it generates estimates of the enhancer-like regulatory potential for each fragment when that fragment is in an unmethylated versus a methylated state (Figure 1A, B). To focus on the CpG sites most likely to be included in DNA methylation studies in humans, we performed custom capture with SeqCap EZ Prime Choice Probes (Roche), targeting all CpG sites on the Illumina Infinium MethylationEPIC array and those likely to be profiled using reduced representation bisulfite sequencing, which enriches for

130 CpG sites near targets of *MspI* restriction enzyme digestion (Figure 1-figure supplement 1).
131 Because of substantial attention to potential environmental and early life effects on DNA
132 methylation at the glucocorticoid receptor gene (*NR3C1*, reviewed in (Liu and Nusslock, 2018)),
133 we also targeted the 6.5 Mb in and flanking *NR3C1*. Finally, to assess background expectations
134 for regulatory and methylation-dependent regulatory activity in the human genome, we targeted
135 a control set of 100,000 loci for capture, chosen at random across the human genome after
136 excluding centromeres, gaps, and uncalled bases in the hg38 genome.
137 We generated an mSTARR-seq library from captured DNA from the GM12878 cell line,
138 followed by transfection into the K562 erythroleukemic cell line and co-purification of plasmid-
139 derived RNA and DNA (6 replicates per condition: methylated versus unmethylated; see
140 Materials and Methods; Supplementary File 1). Based on our minimal criteria for assessment
141 (600 basepair windows where at least half of the plasmid-derived DNA samples had at least 1
142 read covering the window; see Materials and Methods), 90.2% of the human genome was
143 included in the plasmid DNA library purified at the end of the mSTARR-seq experiment (mean
144 sequencing depth per replicate = 30.4 million reads). Within this set, windows were ~15-fold
145 enriched for targeted regions in the genome (Fisher's Exact Test $\log_2$(OR) [95% confidence
146 interval (CI)] = 3.971 [3.934, 4.009], $p < 1.0 \times 10^{-300}$]. Thus, in windows that passed our minimal
147 assessment criteria, we successfully targeted 99.3% of CpG sites on the MethylationEPIC array
148 and 99.4% of sites likely to be included in RRBS libraries. Our results are comparable to
149 published fragment diversity levels achieved with this method (Lea et al, 2018; Figure 1-figure
150 supplement 2). Bisulfite sequencing at the end of the experiment confirmed that DNA
151 methylation levels were substantially higher in the methylated condition samples than in the
152 unmethylated samples, where methylation levels were near zero (mean methylated = 0.885,
153 mean unmethylated = 0.066, Figure 1-figure supplement 3; unpaired t-test: t = -14.66, df =
154 15,124, $p = 2.39 \times 10^{-10}$).
155 To test for regulatory potential, we focused on those windows where at least 3 replicate
156 samples produced at least 1 RNA-seq read in either the methylated condition or in the
157 unmethylated condition (n = 216,091 non-overlapping 600 bp windows, 4.3% of the human
158 genome). These inclusion criteria focused our analysis on the subset of windows where we were
159 able to detect minimal evidence of transcription from the plasmid; the proportion of the human
160 genome showing evidence of regulatory activity is expected to be small based on previous work
161 (e.g., Johnson and colleagues estimated that 0.165% of the human genome had regulatory
162 potential in a genome-wide STARR-seq assay: (Johnson *et al.*, 2018)). Among the regions
163 analyzed here, 3,721 windows (1.7%) showed evidence for regulatory activity, where the amount
164 of RNA generated from a window significantly exceeded the amount of DNA input sequenced
165 for the same window (FDR < 1%; Supplementary File 2). Regions with regulatory activity were
166 enriched for enhancers and active promoters annotated by the ENCODE Consortium for the
167 K562 cell line ($\log_2$(OR) = 0.584 – 3.337; all $p < 1 \times 10^{-3}$; Figure 1C) (ENCODE, 2012; Ernst
168 and Kellis, 2012). In support of assay reproducibility, they also were highly consistent with
169 previous mSTARR-seq data generated in K562 cells using a previously published, independently
170 generated DNA library that we reanalyzed using the current pipeline (overlap among windows
171 with FDR < 1% in each data set analyzed independently: $\log_2$(OR) [95% CI] = 6.212 [6.086,
172 6.440], $p < 1.0 \times 10^{-300}$; Figure 1-figure supplement 4; Supplementary File 3) (Lea *et al.*, 2018).
173 Regions with mSTARR-seq-annotated regulatory activity also exhibited a high degree of
174 consistency between cell types. In a comparison against newly generated mSTARR-seq data
175 from the HepG2 liver cell line, using the same mSTARR-seq library as in the previously

published K562 experiments (Lea *et al.*, 2018), regulatory regions detected in this study were enriched among regulatory regions detected in HepG2 cells ($\log_2$(OR) [95% CI] = 3.534 [3.381, 3.684], p = 5.21 x 10^{-307}; Figure 1-figure supplements 4 and 5; Supplementary File 4). They also overlap with regulatory regions identified in a conventional STARR-seq experiment in A549 lung epithelial cells ($\log_2$(OR) [95% CI] = 2.451 [2.442, 2.461], p < 1.0 x 10^{-300}) (Johnson *et al.*, 2018). Although we prioritized a blood-derived cell line because of the frequency of environmental epigenetic studies done in blood, these results suggest that our findings can be generalized, to some extent, to other cell and tissue types.

Among the 3,721 windows with regulatory activity in either the methylated or unmethylated condition, 1,768 windows (47.5% of regulatory windows; FDR < 1%) were differentially active depending on condition, pointing to DNA methylation-dependent regulatory activity. This result is also concordant when we apply the current pipeline to previously published data from K562s and our new HepG2 data, which exhibit correlated effects of DNA methylation on regulatory activity in the windows examined in both cases (K562: R^2 = 0.286 for 1250 regulatory windows with FDR < 1% in both data sets, p = 3.19 x 10^{-93}; HepG2: R^2 = 0.277 for 511 regulatory windows with FDR < 1% in both data sets, p = 8.87 x 10^{-38} Figure 1-figure supplement 6). Among methylation-dependent regulatory regions, the majority of regions (1744 windows, 98.6%) were more active in the unmethylated condition than the methylated condition. Regulatory windows showing higher activity in the methylated condition (24 windows) were enriched for binding motifs of the transcription factors p53, which has been previously reported to have increased binding affinity to methylated DNA relative to unmethylated DNA (Kribelbauer *et al.*, 2017) ($\log_2$(OR) [95% CI] = 2.352 [0.714, 3.767], p = 2.91 x 10^{-3}; Supplementary File 5), and Tfcp2I1, which has been found to recruit Tet2 to mediate enhancer demethylation (Sardina *et al.*, 2018) ($\log_2$(OR) [95% CI] = 2.615 [0.580, 4.229], p = 6.84 x 10^{-3}).

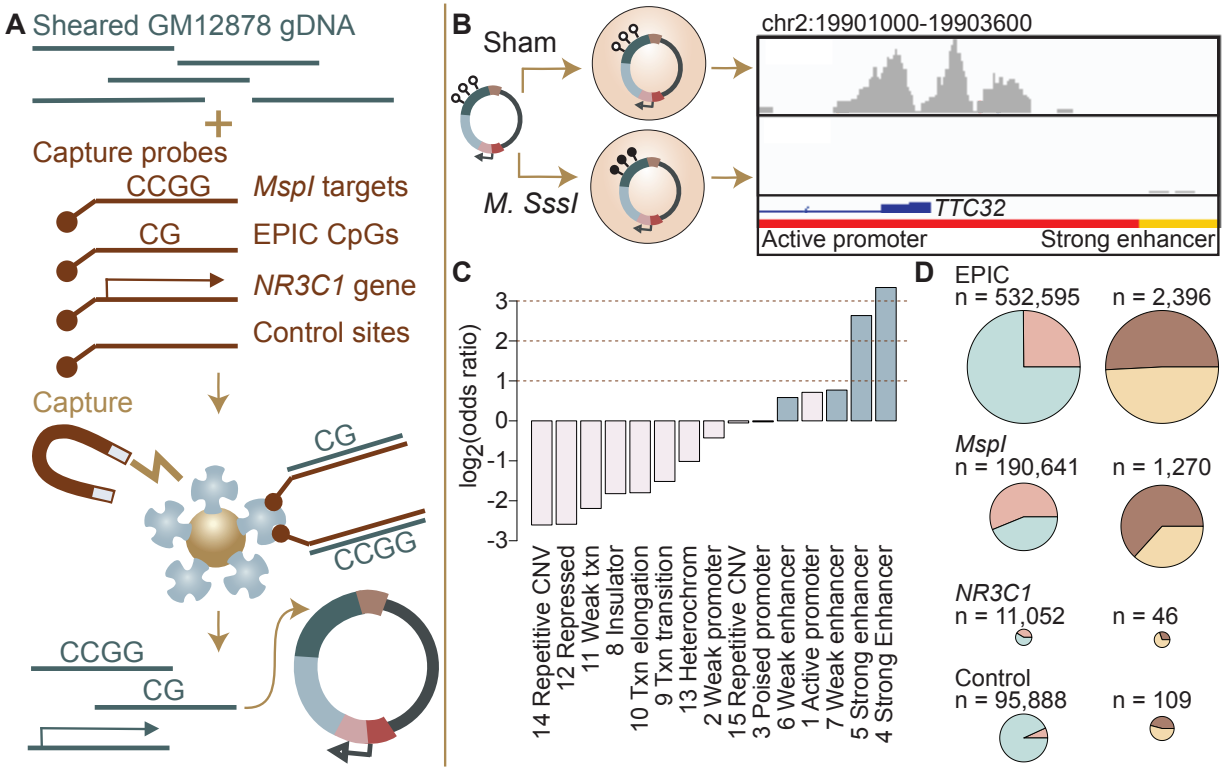

Figure 1. Study design and identification of enhancer activity. (A) Sheared DNA from the GM12878 cell line was subjected to enrichment via capture with probes targeting loci selected in reduced

202 representation bisulfite sequencing (RRBS) workflows (*MspI* targets), CpG sites on the Infinium EPIC
203 array, the gene *NR3C1* and flanking regions, and 100,000 randomly distributed control regions. Library
204 diversity summaries are shown in Figure 1-figure supplement 2. **(B)** Captured loci were cloned into the
205 mSTARR-seq vector, *pmSTARRseq1*, treated with either the CpG methylating enzyme *M. SssI* or a sham
206 treatment, and transfected into K562 cells. Methylation levels of replicate samples are shown in Figure 1-
207 figure supplement 3. Right panel shows an example of DNA methylation-dependent regulatory activity
208 near the first exon of the *TTC32* gene, where the methylation-dependent regulatory element overlaps an
209 active promoter chromatin state (red horizontal bar denotes active promoter as defined by ENCODE
210 (ENCODE, 2012)). **(C)** mSTARR-seq regulatory activity in the baseline condition is strongly enriched in
211 ENCODE-defined enhancers (indicated in blue) and promoters, and depleted in repressed, repetitive, and
212 heterochromatin states. Regions with mSTARR-seq regulatory activity detected in this experiment also
213 significantly overlap with regions with regulatory activity in other mSTARR-seq and conventional
214 STARR-seq datasets (Figure 1-figure supplements 4-6). **(D)** Left column shows, under the baseline
215 condition (i.e. unstimulated cells), the proportion of 600 bp windows that exhibited minimal regulatory
216 activity (at least 3 replicate samples produced at least 1 RNA-seq read in either the methylated condition
217 or in the unmethylated condition) in the mSTARR-seq assay (pink) versus those with detectable input
218 DNA but no evidence of regulatory activity (blue), for windows containing sites from each target set.
219 Note that a single 600 bp window can contain multiple target types (Figure 1-figure supplement 1). Right
220 column shows the proportion of windows with regulatory capacity (i.e., the subset of the windows
221 represented in pink on the left that produce excess RNA relative to the DNA input at FDR < 1%) that are
222 also methylation-dependent (dark brown). Within each column, pie charts are scaled by the total numbers
223 of windows represented.
224
225 **Commonly studied CpG sites are enriched for methylation-dependent regulatory activity**
226 We compared methylation-dependent regulatory activity between CpGs targeted on the
227 EPIC array, CpGs typically profiled in RRBS libraries (i.e., near *MspI* cut sites), the 6.5 Mb in or
228 flanking the glucocorticoid receptor gene *NR3C1*, and the control set of genome-representative
229 loci. As expected, windows that contained EPIC CpG sites, sites associated with RRBS, or that
230 were located in or near *NR3C1* were significantly more likely to show at least some degree of
231 transcriptional activity (i.e., plasmid-derived RNA reads) than the genomic background (i.e.,
232 98,967 randomly distributed loci: see Materials and Methods), and thus were more likely to be
233 included in our analysis set for regulatory activity (EPIC: $\log_2$(OR) [95% CI] = 2.189 [2.152,
234 2.227], $p < 1.0 \times 10^{-300}$; RRBS: $\log_2$(OR) [95% CI] = 4.126 [4.086, 4.163], $p < 1.0 \times 10^{-300}$;
235 *NR3C1*: $\log_2$(OR) [95% CI] = 3.259 [3.193, 3.325], $p < 1.0 \times 10^{-300}$; Figure 1D). However,
236 conditional on minimal transcriptional activity, windows containing EPIC array sites were not
237 more likely to exhibit enhancer-like regulatory activity than background windows of the genome,
238 and RRBS- and *NR3C1*-associated sites were in fact slightly less likely to do so (EPIC: $\log_2$(OR)
239 [95% CI] = 0.112 [-0.168, 0.405], p = 0.47; RRBS: $\log_2$(OR) [95% CI] = -0.493 [-0.779, -0.195],
240 $p = 1.11 \times 10^{-3}$; *NR3C1*: $\log_2$(OR) [95% CI] = -0.730 [-1.263, -0.217], $p = 3.89 \times 10^{-3}$). This
241 result is likely explained by our inclusion criteria, as regions with no evidence for RNA
242 transcription are filtered out prior to analysis.
243 In contrast, among regions with detectable regulatory activity, 63.3% of those containing
244 RRBS-associated CpG sites exhibited methylation-dependent regulatory activity, compared to
245 45.9% of control background loci (RRBS against control: $\log_2$(OR) [95% CI] = 1.025 [0.430,
246 1.624], $p = 4.39 \times 10^{-4}$; Figure 1D; note that of 109 regulatory windows in the control set, 108
247 contain at least 1 CpG, so this difference is not because the control set is CpG-free). Neither
248 windows with EPIC CpGs nor windows in or near *NR3C1* were enriched for methylation-
249 dependent regulatory activity relative to the genomic background (EPIC against control:

250 $\log_2$(OR) [95% CI] = 0.284 [-0.297, 0.871], p = 0.33; *NR3C1* versus control: $\log_2$(OR) [95% CI]
251 = -0.948 [-2.129, 0.178], p = 0.11). Consequently, differential methylation identified through
252 RRBS is more likely to be capable of driving differences in gene regulation, as detectable by
253 mSTARR-seq, than differential methylation elsewhere in the genome. We caution, however, that
254 even among RRBS sites, 98.8% do not occur in regions of the genome with detectable regulatory
255 activity in either the methylated or unmethylated conditions, at least in the K562 cell type, and
256 35.0% of those that fall in putative regulatory elements exhibit no evidence for methylation-
257 dependent activity.
258
259 **Environmental perturbation reveals cryptic regulatory elements and cryptic effects of DNA**
260 **methylation**
261 Enhancer activity can be cell type- or environment-dependent (e.g., (Ostuni *et al.*, 2013;
262 Johnson *et al.*, 2018; Chaudhri *et al.*, 2020). DNA methylation-dependent enhancer activity may
263 show similar context-dependence, thus potentially accounting for the large number of sites that
264 fall in functionally silent regions described above. However, this possibility has not been
265 systematically tested. To do so, we next compared regulatory activity between the baseline
266 unchallenged condition and cells challenged with interferon alpha (IFNA) or dexamethasone
267 (dex) (Figure 2A). Regions that were identified to have regulatory potential in the baseline
268 condition were highly likely to retain regulatory potential after cells were challenged with IFNA
269 or dex (Figure 2-figure supplement 1; IFNA $\log_2$(OR) [95% CI] = 8.639 [8.499, 8.812], $p < 1.0 \times$
270 10^{-300}; dex $\log_2$(OR) [95% CI] = 9.640 [9.483, 9.776], $p < 1.0 \times 10^{-323}$; Supplementary Files 6, 7).
271 However, environmental challenges also revealed thousands of putative regulatory regions that
272 were undetectable at baseline but active post-stimulation (Figure 2B; 1614 IFNA-specific; 1131
273 dex-specific). Of 4,632 IFNA regulatory regions (<1% FDR), 44.1% are not detectable at
274 baseline at a 1% FDR threshold in the baseline condition, and even with a relaxed baseline FDR
275 of 10%, 25.1% remain undetectable. Of 4,217 dex regulatory regions (<1% FDR), 40.2% are not
276 detectable at baseline (1% FDR), and 31.5% remain undetectable at a baseline FDR of 10%.
277 Regulatory windows specific to the IFNA treatment were enriched for 33 transcription
278 factor binding motifs (TFBMs) (Supplementary File 8), with strong enrichments detected for
279 TFBMs involved in innate immune defense in general, and interferon signaling specifically
280 (Figure 2C). For example, the most enriched motif was the canonical DNA target of interferon
281 signaling, known as IFN-stimulated response elements (ISRE; $\log_2$(OR) [95% CI] = 3.158
282 [2.953, 3.358], Bonferroni corrected $p = 7.31 \times 10^{-133}$), followed by binding motifs for several
283 IFN-regulatory factors (IRF1, IRF2, IRF3, IRF4, IRF8; all OR > 1.5 and Bonferroni corrected p
284 $< 1 \times 10^{-15}$) (Chen *et al.*, 2017). Regulatory windows specific to the dex-stimulated condition
285 were significantly enriched for 28 transcription factor binding motifs, including the
286 glucocorticoid response element IR3 and binding motifs of several transcription factors known to
287 interact with or be modulated by the glucocorticoid receptor (AP-1, CEBP:CEBP, CEBP:AP1,
288 JunB, Jun-AP1, GATA1, STAT3, and STAT5; all OR > 1.3, Bonferroni corrected $p < 0.01$;
289 Supplementary File 9) (Cain and Cidlowski, 2017). Results were qualitatively similar if we used
290 a more stringent definition of IFNA-specific and dex-specific regulatory activity (e.g. "IFNA-
291 specific" defined as FDR < 1% in IFNA condition and FDR > 10% in the other two conditions;
292 Supplementary Files 10, 11).
293 To evaluate the relevance of these regions to *in vivo* gene regulation, we also generated
294 matched mRNA-seq data for the endogenous K562 genome from the same experiments. These
295 data showed that expressed genes located closest to mSTARR-seq-annotated, IFNA-specific

enhancers were more strongly upregulated after IFNA stimulation than the set of expressed genes located closest to shared mSTARR-seq-annotated enhancers (i.e., those identified in both the IFNA and at least one other condition, considering genes within 100 kb maximum distance from each enhancer element; unpaired t-test; $t = 3.268$, $df = 601.88$, $p = 1.15 \times 10^{-3}$). We found similar results when using inferred enhancer-gene linkages from the EnhancerAtlas 2.0 (Gao *et al.*, 2016) and restricting the set of IFNA-specific enhancers to those with external experimental support for ISRE binding (n = 1005 windows; ChIP-Seq data from (ENCODE, 2012), relative to all other genes in the gene expression dataset; unpaired t-test; $t = 3.579$, $df = 118.36$, $p = 5.01 \times 10^{-4}$; Figure 2D; Supplementary File 12). Despite a weaker overall gene expression response to dex, genes closest to dex-specific mSTARR-seq enhancers were also more strongly upregulated after dex stimulation than genes near shared enhancers (unpaired t-test; $t = 3.477$, $df = 479.6$, $p = 5.53 \times 10^{-4}$).

For the IFNA challenge, the DNA methylation state of each window appears to play an important role in shaping condition-specific responses to stimulation in the mSTARR-seq data set. Nearly twice as many regulatory windows (81.4%; 1314 of 1614) exhibited methylation-dependent regulatory activity in the IFNA-specific condition than in the baseline or dex-specific condition (47.5% and 48.4% respectively; two-sided binomial test for IFNA compared to baseline: $p = 3.58 \times 10^{-312}$). Further, regulatory regions that harbor TFBMs for TFs central to the interferon response (ISRE, IRF1, IRF2, IRF3, IRF4, IRF8; N = 663 windows) strongly responded to IFNA challenge if in an unmethylated state, but mounted systematically attenuated responses if in a methylated state. As a result, 562 of these 663 windows (84.7%) exhibited significant methylation-dependent regulatory activity and 561 of them (99.8%) were more active in the IFN-challenged state when unmethylated. This pattern is recapitulated when focusing on analyzed windows with external experimental support for ISRE binding (n = 1005 windows; ChIP-Seq data from (ENCODE, 2012)). These windows show no evidence for methylation-dependent regulatory activity in the baseline condition (paired t-test; $t = -0.792$, $df = 1004$, $p = 0.43$), primarily because they show no regulatory activity at all without IFNA stimulation. After IFNA stimulation, though, they exhibit strong methylation-dependence. Specifically, only unmethylated windows are capable of a response (paired t-test; $t = 31.748$, $df = 1004$, $p = 1.02 \times 10^{-153}$; Figure 2E).

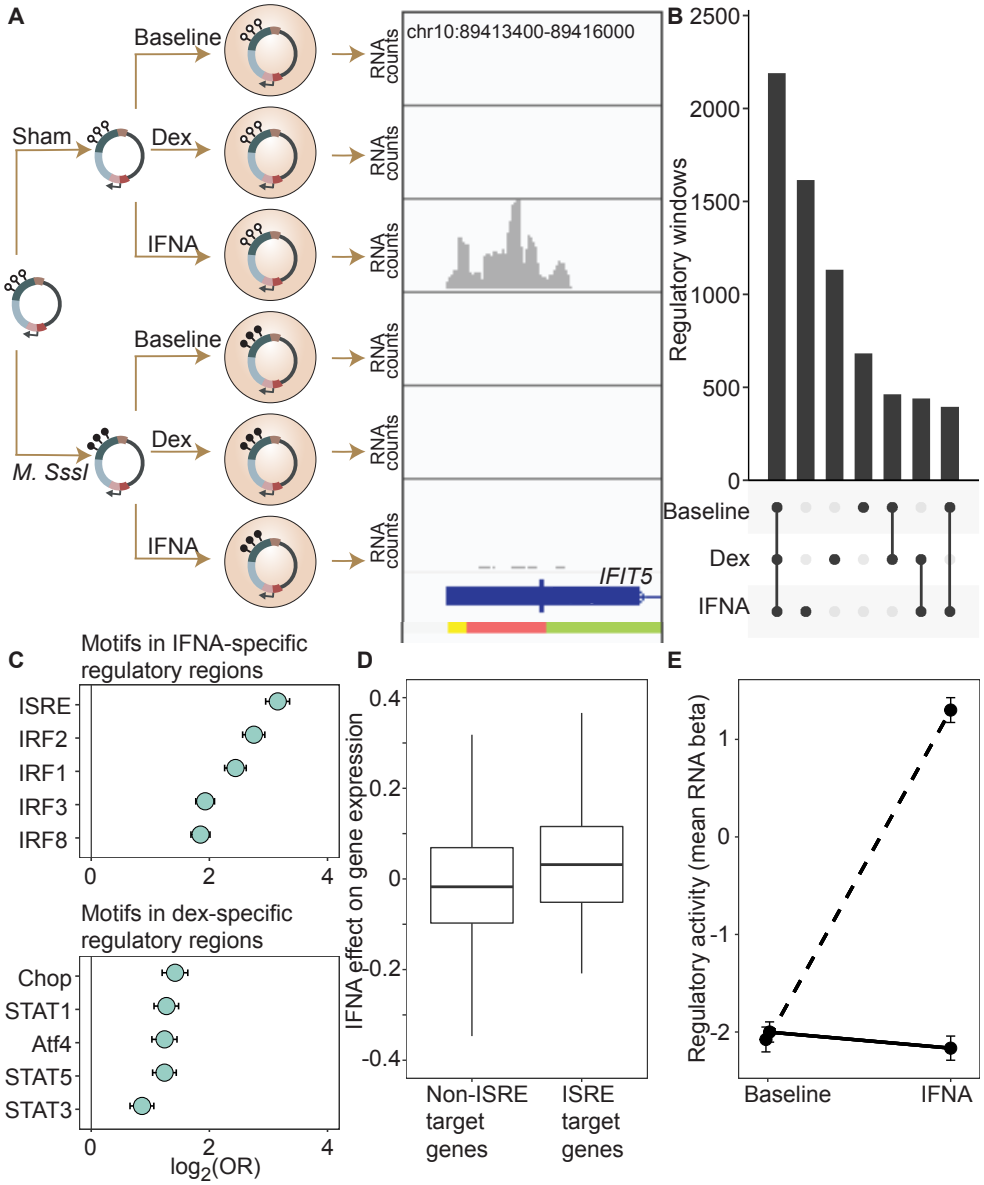

Figure 2. DNA methylation-environment interactions reveal methylation-dependent responses to IFNA and dexamethasone challenge. (A) Full mSTARR-seq design across DNA methylation and challenge conditions. An example of a DNA methylation-environment interaction is shown overlapping the interferon-induced gene *IFIT5* and an ENCODE-annotated weak promoter (pink denotes weak promoter, yellow denotes heterochromatin, and green denotes weak transcription; the endogenous *IFIT5* gene expression response to IFNA in our experiment is shown in Figure 2-figure supplement 2). Three consecutive 600 bp windows have interaction FDR < 1 x 10^{-4} in this region. Panels depict non-normalized, raw read pileups for mSTARR-seq RNA replicates, with all y-axis maximums set to 14000. No methylation-dependent activity is detectable in the baseline condition because this enhancer element is inactive. Upon IFNA stimulation, only unmethylated enhancer elements are capable of responding. **(B)** Upset plot showing shared and unique mSTARR-seq identified enhancer elements across conditions. While many elements are shared, 3426 are unique to a single condition (FET log-odds results for magnitude of overlap are shown in Figure 2-figure supplement 1). **(C)** Top five most enriched transcription factor binding motifs in IFNA- and dex-specific mSTARR-seq enhancers, compared to all windows tested. Whiskers show the standard error. See Supplementary Files 8 and 9 for all enrichment results. **(D)** Genes targeted by ISRE enhancers (ISRE enhancers identified from ENCODE ChIP-seq data;

342 gene targets identified from enhancer-gene linkages from EnhancerAtlas 2.0 (Gao *et al.*, 2016)) that are
343 also identified as IFNA condition-specific mSTARR-seq enhancers show stronger K562 endogenous gene
344 expression responses to IFNA stimulation than non-ISRE targets (unpaired t-test: t = 3.58, df = 118.36, p
345 = 5.01 x 10^{-4}; Supplementary File 12). Each box represents the interquartile range, with the median value
346 depicted as a horizontal bar. Whiskers extend to the most extreme values within 1.5x of the interquartile
347 range. **E)** mSTARR-seq regulatory activity for windows containing ISRE targets (n = 1005 windows)
348 interacts strongly with exposure to IFNA. These windows are capable of mounting a strong response to
349 IFNA stimulation when unmethylated (dashed line; paired t-test: t = 23.02, df = 1004, p = 1.78 x 10^{-94})
350 but not when methylated (solid line; paired t-test: t = -1.74, df = 1004, p = 0.082). Dots show the mean
351 beta corresponding to enrichment of RNA reads versus DNA reads across windows; whiskers show the
352 standard error. Because y-axis values correspond to model estimates, they can be positive (i.e., more
353 mSTARR-seq RNA reads than input DNA reads) or negative values (i.e., fewer mSTARR-seq RNA reads
354 than mSTARR-Seq input DNA reads, indicating no regulatory activity).
355
356 **Methylation levels at mSTARR-seq IFNA-specific enhancers predict the transcriptional**
357 **response to influenza virus in human macrophages**
358 Our findings show that, in the context of mSTARR-seq, pre-existing DNA methylation
359 state can capacitate or constrain the regulatory response to IFNA stimulation. This result
360 suggests that DNA methylation-environment interactions may be an important determinant of
361 gene expression levels *in vivo*. To test this possibility, we drew on matched whole genome
362 bisulfite sequencing (WGBS) and RNA-seq data collected from human monocyte-derived
363 macrophages (n = 35 donors), with and without infection with the influenza A virus (IAV),
364 commonly known as flu (Figure 3A; (Aracena *et al.*, 2022)). We asked whether variation in the
365 gene expression response to flu is predicted by DNA methylation levels in the baseline (non-
366 infected) condition, especially at loci where the response to IFNA is affected by DNA
367 methylation in mSTARR-seq. Importantly, flu and IFNA challenges induce similar innate
368 immune responses (Killip *et al.*, 2015).
369 Within each individual in the macrophage data set, mean DNA methylation levels at
370 baseline significantly predict the mean gene expression response to flu across the full set of
371 mSTARR-seq enhancer windows detected in the IFNA condition (n = 35 individuals at 2769
372 enhancer windows: mean Pearson's r = -0.105 ± 0.006 s.d., all Bonferroni-corrected p < 3 x 10^{-5};
373 Supplementary File 13). This effect is largely driven by the subset of mSTARR-seq IFNA-
374 specific enhancers. Specifically, the correlation between baseline DNA methylation levels and
375 the gene expression response to flu is 3.44-fold stronger in IFNA-specific enhancers than for
376 enhancers identified in both the IFNA condition and at least one other condition (Figure 3B;
377 IFNA-specific enhancers: n = 1033, mean Pearson's r = -0.170 ± 0.009 s.d., all Bonferroni-
378 corrected p < 2 x 10^{-5}; shared enhancers: n = 1736, mean Pearson's r = -0.049 ± 0.01 s.d., all
379 Bonferroni-corrected p > 0.1). These results appear to be driven by strong methylation-
380 dependence in flu-infected cells, as the average within-individual correlation between DNA
381 methylation and gene expression is 2.44 times as large after infection (r = -0.261 ± 0.006) than at
382 baseline (r = -0.106 ± 0.008) in IFNA-specific mSTARR-seq enhancers (Figure 3C;
383 Supplementary File 14).
384 The limited sample size of the macrophage data set makes it better suited for analyses of
385 the overall relationship between DNA methylation and gene expression within an individual,
386 rather than locus-specific analyses of interindividual variation (especially as locus-specific
387 variance in DNA methylation across individuals is low: mean = 0.004, standard deviation =
388 0.008). Nevertheless, across 1382 testable loci (600 bp windows containing at least 1 CpG with

interindividual variance > 0.01), we identified one IFNA-specific, methylation dependent mSTARR-seq enhancer where endogenous variation in DNA methylation levels across individuals clearly predicts the response of the nearest gene's transcriptional response to flu (Figure 3D-E; $p = 6.05 \times 10^{-5}$, q-value = 0.0837; Supplementary File 15). This mSTARR-seq enhancer (chr1:1013400-1014000) overlaps the promoter of interferon-stimulated gene 15 (*ISG15*; Figure 3E), and its average methylation explains 38% of the variance in the *ISG15* transcriptional response to flu across individuals. The magnitude of *ISG15* transcriptional response to flu appears primarily driven by the enhancer's effect on gene expression at baseline. Lower enhancer methylation at baseline is associated with higher *ISG15* expression at baseline, ultimately resulting in a shallower fold change response to flu (Figure 3-figure supplement 1). This example illustrates the value of integrating observational data on DNA methylation and gene expression with mSTARR-seq. The population data support the *in vivo* relevance of the mSTARR-seq data, while the mSTARR-seq data suggest that baseline variation in *ISG15* methylation *in vivo* is causally meaningful to the response to influenza. Notably, *ISG15* plays critical roles in regulating the type I interferon response and modulating host immunity to both viral and bacterial infections (reviewed in (Perng and Lenschow, 2018)).

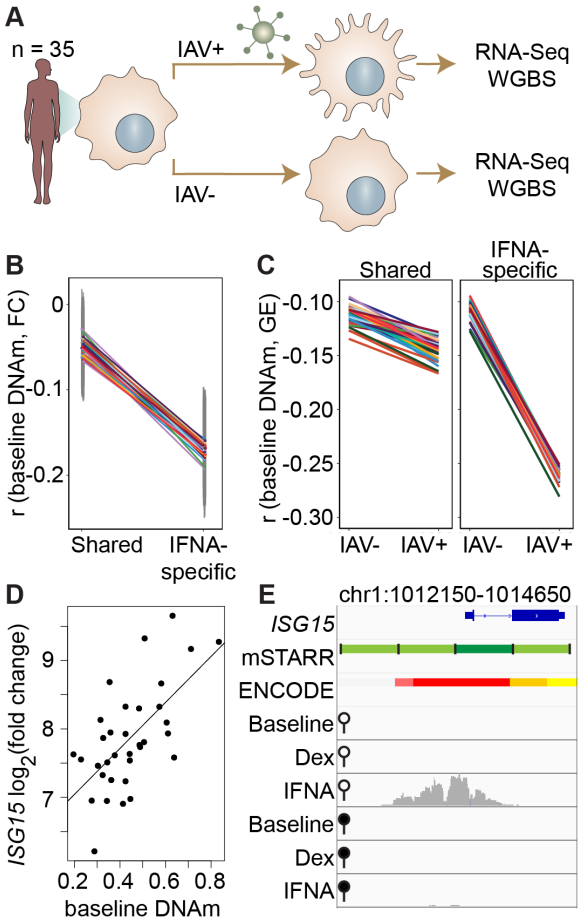

Figure 3. DNA methylation in mSTARR-seq enhancers predicts *in vivo* gene expression in macrophages. (A) Study design of the in *vivo* experiment, in which matched macrophage samples from 35 individuals were either left non-infected or infected with influenza A virus (IAV) for 24 hours and processed for RNA-seq and whole genome bisulfite sequencing (WGBS; (Aracena *et al.*, 2022)). **(B)** Within individuals, DNA methylation (DNAm) levels at mSTARR-seq enhancers in non-infected cells

are negatively correlated with the nearest genes' transcriptional responses to IAV, but only in mSTARR-seq enhancers that were specific to the IFNA condition (IFNA-specific enhancers: n = 1033, mean Pearson's r = -0.170 ± 0.009 s.d., all Bonferroni-corrected $p < 2 \times 10^{-5}$; shared enhancers: n = 1736, mean Pearson's r = -0.049 ± 0.01 s.d., all Bonferroni-corrected p > 0.1). Each colored line represents an individual, and vertical gray lines represent 95% confidence intervals (see Supplementary File 13 for full results). **(C)** The average within-individual correlation (r) between DNA methylation and gene expression (GE) is 2.44 times as large after infection (r = -0.261 ± 0.006) than at baseline (r = -0.106 ± 0.008) in IFNA-specific mSTARR-seq enhancers (right panel), but much less affected by infection at mSTARR-seq enhancers that are shared across conditions (left panel). Each colored line represents an individual (see Supplementary File 14 for full results). **(D)** Across individuals, the *ISG15* transcriptional response to IAV is significantly correlated with average DNAm at the mSTARR-Seq enhancer chr1:1013400-1014000 in non-infected cells ($R^2 = 0.381$, $p = 6.05 \times 10^{-5}$, q = 0.084). Each dot represents an individual (see Supplementary File 15 for full results and Figure 3-figure supplement 1 for condition-specific results). **(E)** The mSTARR-seq enhancer predictive of *ISG15* response to IAV (dark green bar) is located in the active promoter of *ISG15* (as defined by ENCODE (ENCODE, 2012); red denotes active promoter, pink denotes weak promoter, orange denotes strong enhancer, yellow denotes weak enhancer). Three adjacent, methylation-dependent, IFNA-specific mSTARR-seq enhancers were identified (light green), but do not significantly predict *ISG15* response to IAV (q > 10%). The bottom 6 tracks depict non-normalized, raw read pileups for mSTARR-seq RNA replicates in either the unmethylated (open circle) or methylated (filled circle) condition, with all y-axis maximums set to 20,000.

Most CpG sites associated with early life adversity do not show regulatory activity in K562s

Finally, because changes in DNA methylation are of particular interest to research on the biological embedding of early life experience (Hertzman and Boyce, 2010), we tested whether DNA methylation differences associated with early life adversity (ELA) translate to functional effects on gene regulation in the mSTARR-seq data. We first performed a literature search to compile CpG sites that have previously been associated with ELA in humans using the Illumina EPIC array or one of its precursors (Infinium Human Methylation 450K and 27K BeadChips). Our search resulted in a total of 27 studies (Supplementary File 16), which together identified 8,525 unique ELA-associated sites.

For 26 of 27 studies, ELA-associated CpG sites were not more likely to occur within putative regulatory windows (detected in either the methylated condition, unmethylated condition, or both) than background chance (Figure 4). This pattern was qualitatively consistent regardless of whether we considered baseline, IFNA-, or dex-challenged samples (Supplementary File 16). The only exception was for a set of differentially methylated regions in the children of mothers exposed to objective hardship (e.g., living in a shelter, loss of electricity) who were pregnant during or within 3 months of the 1998 Quebec Ice Storm (Cao-Lei *et al.*, 2014). In this study, ELA-associated sites were more likely to fall in windows with regulatory potential in our sample ($\log_2$(OR) [95% CI] = 1.343 [0.715, 1.909], $p = 3.39 \times 10^{-5}$). Among these sites, 53.85% were also detected to have methylation-dependent activity, which is slightly, but not significantly higher than the proportion of methylation-dependent sites on the Illumina Methylation450K chip as a whole ($\log_2$(OR) [95% CI] = 0.884 [-0.338, 2.130], p = 0.16). Consequently, ELA-associated sites in this study were not more likely to exhibit methylation-dependent activity than chance. We speculate that regulatory enrichment in this data set is due to its focus on intermediately methylated CpG sites with substantial interindividual variance in DNA methylation levels, which tends to enrich for enhancer elements. Indeed, ELA-associated sites in this study were more strongly enriched in enhancer regions than the union set of sites in other studies we investigated ($\log_2$(OR) [95% CI] = 1.295 [0.543, 2.015], $p = 6.64 \times 10^{-4}$).

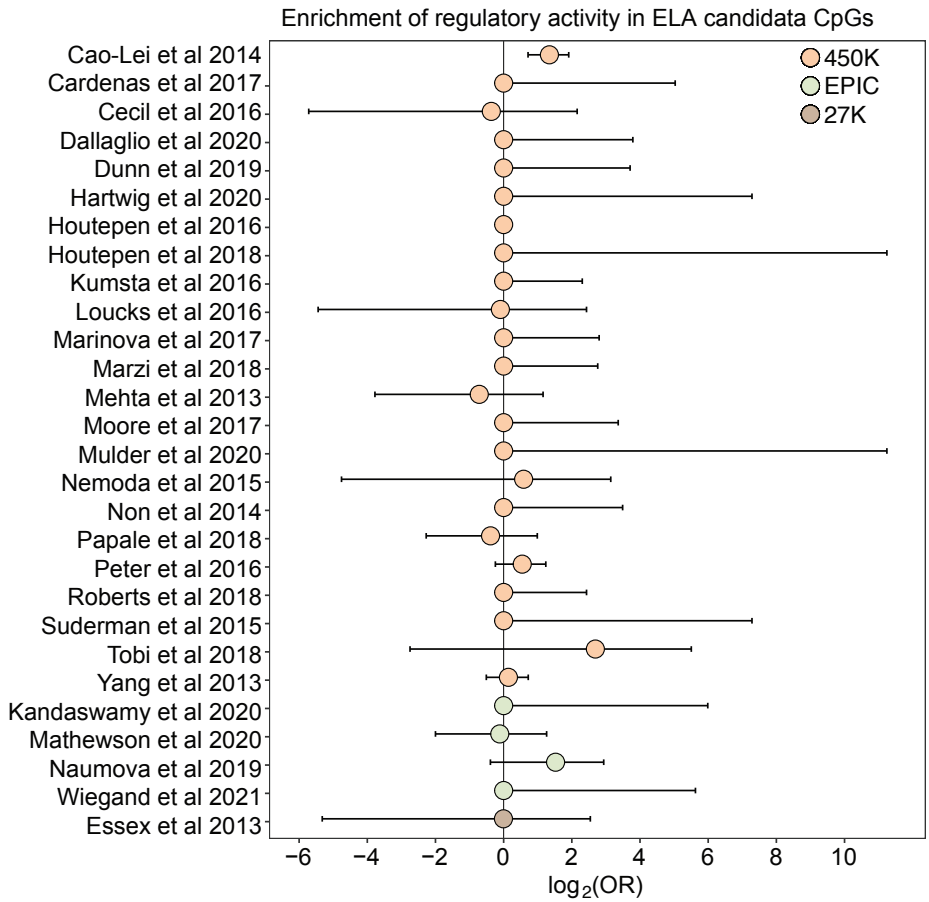

Figure 4. Early life adversity-associated CpG sites are not enriched for mSTARR-seq regulatory activity. Log_2-tranformed odds ratios from Fisher's Exact Tests for enrichment relative to the background set of sites on each array platform, for 27 studies of early life adversity-DNA methylation level correlations (see Supplementary File 16 for full FET results). Whiskers show standard error. Only Cao-Lei *et al*., 2014 shows significant enrichment for regulatory activity (log_2(OR) [95% CI] = 1.343 [0.715, 1.909], p = 3.39 x 10^{-5}), but these sites are not more likely to exhibit methylation-dependent activity than expected by chance (log_2(OR) [95% CI] = 0.884 [-0.338, 2.130], p = 0.16). For details on the source tissue and measures of ELA, see Figure 4-figure supplement 1.

Discussion

Using mSTARR-seq, we assessed the functional role of DNA methylation across more than 99% of CpG sites assessed by two commonly used methods to measure methylation (the EPIC array and RRBS). Compared to our previous work, we identify a higher rate of methylation-dependence in the present data set (47.5% of analyzed windows in the current data set versus 10% of analyzed windows from (Lea *et al.*, 2018) when we apply the current pipeline to analyze both datasets). This difference likely stems from lower variance between replicates in the present study, which increases power. Thus, our findings reveal that DNA methylation often significantly attenuates regulatory activity in K562 enhancer and promoter elements.

The results also support the idea that CpG sites identified by environment-DNA methylation association are a mixed bag. For example, 98% of CpG sites associated with early life adversity in the literature fell in windows with no discernable regulatory potential in K562

479 cells, irrespective of their methylation status. Our findings suggest that many ELA-associated
480 sites may be better treated as passive biomarkers of exposure rather than links on the causal
481 pathway between early life disadvantage and later life health outcomes. However, they also
482 dovetail with work supporting the importance of CpG sites within enhancer elements in
483 responding to environmental perturbations (Pacis *et al.*, 2015; Husquin *et al.*, 2018). Given that
484 the repertoire of poised and active enhancers often differs across cell types and cellular states,
485 expanding experimental approaches like mSTARR-seq to other contexts can therefore serve a
486 valuable role in prioritizing CpG sites identified in observational studies of differential
487 methylation.
488 Indeed, one of the most interesting findings from our analysis is the observation that
489 DNA methylation-environment interactions are widespread in the human genome. Across
490 thousands of genomic regions, both regulatory activity and methylation-dependent effects on
491 regulatory activity were only detectable upon stimulation, consistent with a model in which DNA
492 methylation contributes to epigenomic priming by modulating responsivity to environmental
493 stimuli (Kamada *et al.*, 2018; Sun and Barreiro, 2020). In support of this idea, IFNA-specific
494 enhancers detected in mSTARR-seq are able to nonrandomly identify collections of loci in the
495 genome where baseline DNA methylation also predicts the endogenous gene expression
496 response to flu infection (Figure 3B-C). This relationship is easier to discern in within-individual
497 comparisons across loci than in locus-by-locus analyses of interindividual variation. However,
498 we were also able to pinpoint one specific gene, *ISG15*, in which baseline DNA methylation
499 explains a large fraction of population variation in the gene expression response to flu (Figure
500 3D-E). Notably, the effect size for *ISG15* is very large, accounting for over a third of total
501 variance in the fold-change gene expression response to flu. Our results suggest that mSTARR-
502 seq could therefore help identify additional *in vivo* DNA methylation-environment interactions,
503 given a larger sample size of individuals and power to detect smaller effects.
504 Applying mSTARR-seq in additional cell types may therefore help resolve whether DNA
505 methylation is responsible for exaggerated transcriptional responses to repeated challenges, as
506 previously suggested for glucocorticoid exposure in hippocampal progenitor cells (Provençal *et*
507 *al.*, 2020), or whether differential methylation after pathogen infection contributes to the
508 emerging paradigm of "trained immunity" in innate immune cells (reviewed in (Fanucchi *et al.*,
509 2021)). More generally, while our findings agree with the idea that many differences in DNA
510 methylation—even extreme ones (~0% versus ~100%) like those tested here—are silent with
511 respect to transcription factor binding and gene expression (e.g., (Maeder *et al.*, 2013; Kreibich
512 *et al.*, 2023)), they also suggest that the functional importance of DNA methylation is likely to be
513 underestimated without considering its interaction with the cellular environment.
514
515 **Materials and Methods**
516 *DNA capture and mSTARR-Seq*
517 We used the DNEasy Blood and Tissue Kit (Qiagen) to extract 5 ug DNA from the
518 GM12878 lymphoblastoid cell line. We sheared the extracted DNA on a Covaris S2 with the
519 following parameters: intensity: 3; duty cycle: 5%; cycles/burst: 200: treatment time: 40 seconds;
520 temperature: 4C; intensifier: yes. We then performed agarose gel size selection of ~600-700 bp
521 DNA fragments followed by purification with the Qiaquick Gel Extraction Kit (Qiagen). We
522 note that we intentionally targeted longer fragments (~600-700 bp) than those targeted in (Lea *et*
523 *al.*, 2018) (~300-700 bp) because our previous work showed that longer fragments are more
524 likely to drive regulatory activity (Lea *et al.*, 2018).

We used Roche's NimbleDesign Software to design probes to capture the following genomic regions: (i) EPIC CpGs targeted by the Illumina Infinium MethylationEPIC microarray (862,831 CpGs); (ii) predicted CpG cut sites from an *in silico Msp1* digest of the hg38 genome, followed by *in silico* size selection to 100-500 bp, which together simulates the first step in reduced representation bisulfite sequencing protocols (318,929 CpGs); (iii) 6.5 Mb centered around the *NR3C1* glucocorticoid receptor gene; and (iv) 100,099 loci included as a control for genomic background that were randomly distributed across the hg38 human genome, excluding centromeres, gaps, and Ns. Although the Y chromosome was included during the design of control loci, we excluded the Y chromosome in analyses, resulting in 99,999 control loci which fell into 98,967 unique 600 bp windows. Of these 98,967 windows, 94,679 contained CpG sites and 4,288 did not, reflecting the sequence composition of the human genome as a whole. We note that a single 600 bp genomic window could simultaneously include EPIC CpGs, *Msp1* CpG cut sites, the *NR3C1* region, or control sites (i.e., assignment of windows to these compartments are not mutually exclusive; Figure 1-figure supplement 1).

We then captured target regions from the sheared GM12878 DNA using SeqCap EZ Prime Choice Probes (Roche), following the SeqCap EZ HyperCap protocol version 2.3. We performed two capture reactions. We used 6 cycles for the Pre-Capture LM-PCR program and 16 cycles for the Post-Capture LM-PCR program. For the Post-Capture LM-PCR reaction, we used the mSTARR_primerF2 and mstarr_primerR2 primers from (Lea *et al.*, 2018) to prepare the DNA for ligation into the mSTARR plasmid. The resulting captured DNA was used as input for the mSTARR-seq protocol (Lea *et al.*, 2018), beginning at the mSTARR-seq published protocol step "Generate linearized mSTARR backbone for large-scale cloning".

We performed 4 and 6 replicate Gibson assemblies and transformations for the first and second capture reactions, respectively. We then sequenced each transformation replicate on a MiSeq to measure library diversity per replicate, with the following modifications to the published mSTARR-seq protocol: we used 25 ul Kapa HiFi HotStart ReadyMix instead of 25 ul NEB Q5 Hot start master mix, with the following cycle program: 98 C for 45 sec, 12 cycles of 98 C for 15 seconds, 60 C for 30 seconds, and 72 C for 60 seconds, followed by a final extension at 72 C for 5 minutes. We measured library diversity of each transformation using the ENCODE Project's PCR bottleneck coefficient (PBC), which is the percentage of non-duplicate mapped reads from the total number of mapped reads (Landt *et al.*, 2012) (Supplementary File 17). We pooled the ten transformations by weighting their molarities according to the PBCs to create the final library. We then performed 8 re-transformations to expand the pooled library.

Replicate methyltransferase reactions and parallel mock methyltransferase reactions, in which the *M. SssI* enzyme was replaced with water, were performed in 500 ul reactions, cleaned with Ampure beads, and then pooled. The methylated DNA library and unmethylated DNA library were each transfected into 18 replicate T75 flasks, each containing 12 million K562s, with Lipofectamine 3000 (ThermoFisher Scientific) following the manufacturer's instructions. 42 hours post-transfection, replicates were treated with 2,000 U/mL IFNA2b (Thermo Fisher Scientific), 1 uM dex (Sigma-Aldrich), or vehicle control (media). 48 hours post-transfection (6 hours post-treatment), cells were harvested for mSTARR-seq sequencing library generation. At harvest, 5 x 10^5 cells were aliquoted separately into Buffer RLT to measure endogenous RNA response to treatment, and 2 million cells were aliquoted for plasmid DNA extraction to measure input DNA in each replicate. mSTARR RNA-seq and DNA-seq libraries were generated following (Lea *et al.*, 2018). To measure endogenous gene expression from K562s in each

570 condition, we extracted RNA from the separately aliquoted cells using the Qiagen RNEasy kit
571 and prepared RNA-seq libraries using the NEBNext Ultra II RNA Library Prep Kit for Illumina.
572
573 *Comparison of mSTARR MD regulatory activity across cell types and experiments*
574 To assess cell type-specificity of methylation-dependent regulatory activity, we
575 transfected the mSTARR-seq library from (Lea *et al.*, 2018), comprised of 1:3 sheared genomic
576 DNA:*MspI*-digested DNA, into the HepG2 cell line. For the HepG2 experiment, we performed
577 one methyltransferase reaction and one sham methyltransferase reaction. Transfections were
578 performed with Lipofectamine 3000 (ThermoFisher Scientific) following the manufacturer's
579 instructions, with reagent quantities scaled to the following per replicate: 6.9 million HepG2
580 cells, 46 ug of DNA, 138 ul of Lipofectamine 3000, and 180 ul of P3000 (transfection enhancer
581 reagent). We performed all regulatory and MD regulatory analyses of HepG2 cells, as well as
582 analyses of K562s from a previously published smaller mSTARR-seq experiment (Lea *et al.*,
583 2018), following the same bioinformatics pipeline used for our main K562 experiment, described
584 below. To compare against previously published STARR-seq data in A549 cells, we identified
585 the union set of all regulatory peaks identified across six replicate STARR-seq experiments
586 collected at time point 0 in (Johnson *et al.*, 2018). To test for significant overlap between the
587 current K562 results and the other three data sets, we used Fisher's exact tests against a
588 background set of windows tested in both the current K562 experiment and each of the other data
589 sets.
590
591 *mSTARR-seq regulatory and MD regulatory analyses*
592 mSTARR RNA-seq and DNA-seq libraries were sequenced on the Illumina NovaSeq
593 platform as 100 basepair, paired-end reads (Supplementary File 1). Reads were trimmed with
594 Trim Galore (version 0.6.4) (Krueger, 2015) to remove basepairs at the ends of reads with Phred
595 scores less than 20 and stretches of 2 or more basepairs that matched adapter sequences.
596 Trimmed reads with a minimum length of 25 basepairs were retained. We mapped reads using
597 *bwa* (version 0.7.12) (Li and Durbin, 2009) using default settings. We retained read pairs that
598 mapped to a single best location using the *samtools* (version 1.3.1) (Li *et al.*, 2009) package
599 'view' command with options -q 10 -f 0x2. We segmented the genome into 600 bp, non-
600 overlapping windows, and used the bedtools (version 2.25.0) (Quinlan and Hall, 2010) *coverage*
601 function to count the number of RNA and DNA fragments overlapping each 600 bp window. We
602 chose 600 bp for the genomic window size to accommodate our library's DNA fragment size
603 (600-700 bp; Supplementary File 1), and because using smaller windows resulted in the
604 identification of many adjacent windows as separate regulatory elements when they likely
605 represent a single true enhancer (the median length of ENCODE-annotated enhancers is 600 bp).
606 For each of the 3 treatment conditions (baseline, IFNA, and dex), we reduced our dataset
607 to windows for which at least three DNA samples in the methylated condition and three DNA
608 samples in the unmethylated condition (i.e., 6 DNA samples total), and three RNA samples in
609 *either* the methylated or unmethylated condition, had nonzero counts. One mSTARR RNA-seq
610 sample in the baseline condition (sample ID L31250) was removed from further analysis because
611 it had an unusually high proportion of zero counts in the testable windows; the corresponding
612 paired DNA sample was therefore also removed prior to analysis (Supplementary File 1). Next,
613 we retained only windows that showed high repeatability across DNA samples, following (Lea *et*
614 *al.*, 2018). In brief, for each window we calculated the pairwise difference of read abundance for
615 every pair of samples and created a distribution of all pairwise differences; windows were

removed if at least 25% of pairs fell outside the central 90th percentile of the distribution (37,410 windows, 14.8% of the overall data set). On this reduced data set of testable windows, we performed voom normalization using the limma (version 3.44.3) *voomWithQualityWeights* function (Smyth, 2005; Law *et al.*, 2014), with methylation status included as a covariate in the design. We then used the *limma* function *lmFit* to apply the following model for each window:

$$y_i = \mu + m_i\beta_1 + s_i\beta_2 * I(m = 0) + s_i\beta_3 * I(m = 1) + \varepsilon_i$$

where y_i is the vector of normalized counts for n = 24 samples (12 RNA and 12 DNA samples; 22 samples for the baseline condition); μ is the intercept; m_i is methylation condition (0 = unmethylated; 1 = methylated) and β_1 its effect size; and I is an indicator variable in which β_2 and β_3 are the effects of sample type (s_i; 0 = DNA; 1 = RNA) in the unmethylated (m = 0) and methylated conditions (m =1), respectively. ε_i is the residual error.

To estimate the false discovery rate for identifying windows with regulatory activity (in either the methylated or unmethylated condition, or both), we compared the observed results to empirical null distributions generated using 100 permutations of RNA/DNA labels within each pair of samples. Unlike in the real data, in which most windows show a strong bias towards more reads in the DNA condition (because most windows exhibit no regulatory activity), permuted data results in relatively balanced effect sizes. Using the overall distribution of test statistics to construct the null therefore substantially inflates the number of significant windows, but specifically because most windows have systematically *less* activity in the RNA condition than the DNA condition, not more (the direction of interest). Consequently, for each permutation, we subsampled N windows with a positive sample type beta (corresponding to larger read counts in RNA samples versus DNA samples) in either the methylated condition, unmethylated condition, or both. Here, N is the number of windows with a positive sample type beta in the observed data. The p-values from these windows were used to generate the empirical null. To define putative enhancer elements, we used an FDR cutoff of 1%.

To identify methylation-dependent enhancer activity, we focused on the windows that exhibited a positive sample type beta in either the methylated or unmethylated condition (or both) and tested for significant differences between β_2 and β_3 in the equation above (i.e., an interaction effect between RNA/DNA condition and the methylated/unmethylated condition). To estimate the false discovery rate for identifying methylation-dependent windows, we re-ran our main nested model on the same 100 sets of N windows each, in this case permuting methylation condition (unmethylated versus methylated) across sample pairs to generate the empirical null for the interaction effect of sample type (RNA versus DNA) * methylation condition (methylated or unmethylated). To define methylation-dependent regulatory elements, we again used an FDR cutoff of 1%.

Enrichment of transcription factor binding motifs

To identify enrichment of potential transcription factor binding sites in the methylated condition, we used HOMER and motifs defined in the HOMER database (Heinz *et al.*, 2010) and the baseline treatment dataset to compare motifs within regulatory regions in the methylated condition, relative to motifs across all regulatory regions.

To identify potential transcription factor binding sites in windows with condition-specific regulatory or methylation-dependent regulatory activity, we first identified regions showing regulatory activity uniquely in the dex or IFNA conditions relative to both other conditions

661 (based on an FDR of 1% to define regulatory activity). We used HOMER and motifs defined in
662 the HOMER database to test for enrichment of transcription factor binding motifs within
663 windows showing condition-specific regulatory activity relative to all windows tested for
664 regulatory activity in that condition. We set a threshold of Bonferroni-corrected p-value < 0.01 to
665 identify significantly enriched binding motifs.
666
667 *Endogenous gene expression response of K562s to dex and IFNA*
668 Endogenous RNA-seq libraries were sequenced on an Illumina NovaSeq 6000 S1 flow
669 cell as 100 base pair, paired-end reads. Reads were trimmed with Trim Galore (Trim Galore
670 version 0.6.4_dev; Cutadapt version 2.3) to remove basepairs with a Phred score less than 20,
671 and end sequences that matched at least two basepairs of the adapter sequence. Only trimmed
672 reads longer than 25 basepairs were retained. We used the STAR package (version 2.5.0) (Dobin
673 *et al.*, 2013) two-pass mapping to map the filtered reads to the hg38 genome. We retained
674 uniquely mapped reads by filtering the output SAM file to keep reads with MAPQ = 255. We
675 then used *htseq* (version 0.6.0) (Anders *et al.*, 2014) to quantify read counts per gene. We only
676 retained genes that had TPM > 3 in at least 3 of 6 samples in at least one of the three conditions
677 (baseline, IFNA, or dex). Only protein-coding genes were retained for final analysis, resulting in
678 a total of 10,676 testable genes.
679 We performed differential expression analysis separately for IFNA and dex, by subsetting
680 the data to the IFNA and baseline samples, or subsetting the data to the dex and baseline
681 samples. For each subset, we *voom* normalized the data (Law *et al.*, 2014), and used the *limma*
682 (Smyth, 2005) function *lmFit* to model the normalized gene expression as a function of
683 treatment, controlling for the percent of reads mapping to annotated features (to account for
684 technical variation in the efficiency of RNA purification during library prep) and methylation
685 condition for the associated sample. We calculated the FDR using the q-value approach of
686 (Storey and Tibshirani, 2003), based on an empirical null distribution that was derived from 100
687 permutations of treatment condition in the model.
688 To test whether genes were more responsive to IFNA stimulation if they were predicted
689 targets of IFNA-specific ISRE enhancers, we first used the bedtools *intersect* function to identify
690 the union set of ChIP-seq peaks for STAT1 and STAT2 (two of the three components of the
691 ISGF3 transcription factor that binds ISRE motifs; ENCODE accession numbers
692 ENCFF478XGE and ENCFF394KTR; ChIP-Seq data were not available for the third ISGF3
693 component, IRF9). We then reduced these regions to those showing significant, IFNA condition-
694 specific regulatory activity in the mSTARR-seq dataset (FDR < 1%). We used K562 enhancer-
695 gene links from EnhancerAtlas 2.0 (Gao *et al.*, 2016) to link the resulting IFNA-specific ISRE
696 enhancers to their target genes. Finally, we performed a two-sided, unpaired t-test to compare the
697 endogenous expression responses to IFNA for genes associated with putative IFNA-specific
698 ISRE enhancers relative to genes that are not associated with IFNA-specific ISRE enhancers.
699
700 *Endogenous gene expression and methylation in human macrophages*
701 To assess effects of DNA methylation-environment interactions on gene expression *in*
702 *vivo*, we evaluated endogenous methylation and gene expression from matched whole genome
703 bisulfite sequencing (WGBS) and RNA-seq data collected from human monocyte-derived
704 macrophages (n = 35 donors), with and without infection with the influenza A virus (IAV;
705 (Aracena *et al.*, 2022)). Unsmoothed methylation counts were obtained for 19,492,906 loci in
706 both non-infected and IAV-infected samples (total n = 70) as described (Aracena *et al.*, 2022).

707 We filtered loci to require coverage of ≥ 4 sequence reads in at least half of the non-infected or
708 IAV-infected samples. In the RNA-seq dataset for the same 35 individuals, we excluded any
709 genes that did not have an average RPKM > 2 in non-infected or IAV-infected samples. This
710 resulted in a total of 19,041,420 CpG sites and 14,122 genes used in downstream analyses.
711 We calculated normalization factors using calcNormFactors in edgeR (v 3.28.1)
712 (Robinson *et al.*, 2010) to scale the raw library sizes. We then used the voom function in limma
713 (v 3.42.2) (Smyth, 2005; Ritchie *et al.*, 2015) to apply the normalization factors, estimate the
714 mean-variance relationship, and convert raw read counts to log(CPM) values. Sequencing
715 batches were regressed out using ComBat from the sva Bioconductor package (v 3.34.0) (Leek *et*
716 *al.*, 2012), which fit a model that also included age (mean centered) and admixture. We
717 subsequently regressed out age effects using limma. Individual-wise fold-change (FC) matrices
718 were built by subtracting non-infected counts from IAV-infected counts for each individual using
719 weights calculated as in (Harrison *et al.*, 2019; Aracena *et al.*, 2022).
720 For comparison of the mSTARR-seq dataset to the dataset from (Aracena *et al.*, 2022),
721 GrCh38/hg38 coordinates were lifted over to GRCh37/hg19 using the UCSC liftOver tool. We
722 required a 0.95 minimum ratio of bases that remap, excluded loci that output multiple regions,
723 set the minimum hit size in query to 0, and set the minimum chain size in the target to 0. The
724 GRCh37/hg19 coordinates were used in the following analyses.
725 We first sought to assess, within each of the 35 individuals, the correlation between
726 mSTARR-seq enhancer methylation levels at baseline (i.e., in non-infected cells) and
727 transcriptional responses of their nearest genes to IAV. To find overlaps between enhancer
728 regions and CpG loci, we used the *bedtools* intersect function (v2.29.1) with the "left outer join"
729 option. For each 600 bp mSTARR-seq enhancer region in each individual, we calculated the
730 mean methylation level across all overlapping CpGs. Each enhancer was linked to its nearest
731 gene, with a maximum distance of 100 kb, as described above. If an enhancer had multiple
732 linked genes (e.g., an enhancer that overlapped more than one gene), we took the mean
733 transcriptional response of all linked genes. For each individual, we calculated the Pearson's
734 correlation coefficient (r) between the DNA methylation levels within the mSTARR-seq-defined
735 enhancer windows, in non-infected cells, and transcriptional responses of their linked genes to
736 IAV infection. We also investigated the correlation between mean mSTARR-seq enhancer
737 window methylation and gene expression *within* non-infected and flu-infected samples
738 separately.
739 Finally, for each mSTARR-seq enhancer-gene pair, we sought to test the extent to which
740 average methylation level in the enhancer in non-infected samples explained the gene's
741 transcriptional response to IAV, across individuals. Here, we calculated the average CpG
742 methylation level for each 600 bp enhancer, after excluding CpGs with methylation variance less
743 than 0.01 across individuals. Thus, enhancers that did not contain any CpGs with appreciable
744 interindividual variation in DNA methylation levels were excluded from the analysis. This
745 filtering step resulted in 1,382 enhancer-gene pairs for this analysis. For each enhancer-gene pair,
746 we calculated the Pearson's correlation coefficient (and R^2) between the average methylation
747 level of the enhancer and the transcriptional response of the linked gene. P-values were corrected
748 for multiple hypothesis testing using the q-value method in R (Storey and Tibshirani, 2003).
749
750 *CpG methylation associated with early life adversity*
751 We performed a literature search to identify studies for which CpG methylation
752 differences have been linked to adverse conditions during early life. We considered all journal

articles that contained the words “early life adversity” and “Infinium” on https://scholar.google.com on May 10, 2021, which produced 269 results. We required that the study evaluated CpG methylation using an Illumina Infinium array (27K, 450K, or EPIC), and that the article provided Infinium CpG probe IDs or CpG genomic coordinates of candidate CpGs. Articles that reported no significant CpG sites, but still reported “top” CpG sites, were retained. Articles that performed analyses to identify differentially methylated regions (DMRs; as opposed to CpG site-by-site analysis), and then reported individual CpG sites within the candidate DMRs, were retained. We considered early life adversity to encompass both social and nonsocial sources of environmental adversity (e.g., exposure to severe weather), any time from prenatal development to 18 years of age. We did not impose criteria for cell type or subject age at time of sampling. See Figure 4-figure supplement 1 and Supplementary File 12 for a summary of the resulting studies.

For each study dataset, we performed a Fisher’s exact test to test whether ELA candidate sites, relative to the total set of CpG sites on the Illumina array used in that study (450K, EPIC, or 27K array), were enriched in the mSTARR-seq regulatory windows we identified in the baseline, dex, or IFNA condition.

Acknowledgments

We thank B.J. Nielsen, Tawni Voyles, and Tina Del Carpio for their contributions to data generation, Terrie Moffitt and the Reddy lab at Duke University for project feedback, Graham Johnson for sharing the A549 data, Courtney Karner for use of equipment, and Xiang Zhou for constructive advice on statistical modeling. This study was supported by the National Institutes of Health (R01HD088558 to J.T. and F32HD095616 to R.A.J.), the Canadian Institutes for Advanced Research Child Brain and Development Program, a Sloan Foundation Early Career Research Fellowship to J.T., and a Foerster-Bernstein Postdoctoral Fellowship to R.A.J. High-performance computing resources were supported by the North Carolina Biotechnology Center (Grant Number 2016-IDG-1013 and 2020-IIG-2109).

Data Availability

mSTARR-seq RNA and DNA sequencing data generated in this study for K562 and HepG2 cells are available in the NCBI Sequence Read Archive (SRA; BioProject accession number PRJNA922490). K562 endogenous RNA-seq data are available in the NCBI Gene Expression Omnibus (GEO series accession GSE222643). The previously published data from (Lea *et al.*, 2018) used in this study are available in NCBI’s SRA accession number SRP120556. The previously published A549 data from (Johnson *et al.*, 2018) were kindly provided by Graham Johnson. The sequencing data for the macrophage RNA-seq and WGBS datasets are available at the European Genome-phenome Archive (EGA) under accession numbers EGAD00001008422 and EGAD00001008359, respectively. The zenodo repository at https://zenodo.org/record/7949036#.ZGZ5UnbMJq9 provides the code used for analyses, as well as track files (compatible with the UCSC genome browser) for mSTARR-seq hg38 windows with regulatory activity, and windows with methylation-dependent regulatory activity, in all three conditions (baseline, IFNA, and dex). The mSTARR-seq plasmid, *pmSTARRseq1* is available through AddGene.

Figure Supplements

Figure 1-figure supplement 1. Overlap of target genomic regions with each other.

Figure 1-figure supplement 2. mSTARR-seq library diversity.

Figure 1-figure supplement 3. Methylation levels of mSTARR-seq DNA, pre- and post-transfection.

Figure 1-figure supplement 4. Overlap of regulatory activity across datasets.

Figure 1-figure supplement 5. Library diversity and regions of regulatory activity in HepG2 cells.

Figure 1-figure supplement 6. Methylation-dependent regulatory activity across datasets.

Figure 2-figure supplement 1. Regulatory activity and effects of methylation across environmental conditions.

Figure 2-figure supplement 2. *IFIT5* endogenous gene expression is responsive to IFNA stimulation.

Figure 3-figure supplement 1. Relationship between baseline methylation in the mSTRR-seq annotated enhancer chr1:1013400-1014000 and *ISG15* gene expression in non-infected and IAV-infected macrophages.

Figure 4-figure supplement 1. Summary of early-life adversity (ELA) studies.

Supplementary Files

Supplementary File 1. Table summarizing the K562 mSTARR-seq DNA and RNA libraries generated in this study.

Supplementary File 2. Table of results from the model testing for methylation-dependent regulatory activity in K562 cells at baseline.

Supplementary File 3. Table of results from the model testing for methylation-dependent regulatory activity in K562 cells at baseline condition using the dataset from (Lea *et al.*, 2018).

Supplementary File 4. Table of results from the model testing for methylation-dependent regulatory activity in HepG2 cells at baseline.

Supplementary File 5. Table of enrichment results of transcription factor binding motifs for regulatory windows with higher activity in the methylated relative to the sham condition.

Supplementary File 6. Table of results from the model testing for methylation-dependent regulatory activity in K562 cells stimulated with IFNA.

Supplementary File 7. Table of results from the model testing for methylation-dependent regulatory activity in K562 cells stimulated with dex.

845
846 Supplementary File 8. Table of enrichment results of transcription factor binding motifs for
847 regulatory windows specific to the IFNA treatment (<1% FDR in IFNA and >1% FDR in
848 baseline and Dex).
849
850 Supplementary File 9. Table of enrichment results of transcription factor binding motifs for
851 regulatory windows specific to the Dex treatment (<1% FDR in Dex and >1% FDR in baseline
852 and IFNA).
853
854 Supplementary File 10. Table of enrichment results of transcription factor binding motifs for
855 regulatory windows specific to the IFNA treatment (<1% FDR in IFNA and >10% FDR in
856 baseline and Dex).
857
858 Supplementary File 11. Table of enrichment results of transcription factor binding motifs for
859 regulatory windows specific to the Dex treatment (<1% FDR in Dex and >10% FDR in baseline
860 and IFNA).
861
862 Supplementary File 12. Table of results from the model testing for the K562 endogenous gene
863 expression response to IFNA.
864
865 Supplementary File 13. Table of Pearson's correlation results, within individuals, between
866 mSTARR-seq enhancer DNA methylation in non-infected macrophages and transcriptional
867 response of nearest genes upon IAV infection.
868
869 Supplementary File 14. Table of Pearson's correlation results, within individuals, between
870 mSTARR-seq enhancer DNA methylation in non-infected macrophages and gene expression
871 level in non-infected or IAV-infected macrophages.
872
873 Supplementary File 15. Table of Pearson's correlation results, across individuals, between
874 mSTARR-seq enhancer DNA methylation in non-infected macrophages and transcriptional
875 response of nearest genes upon IAV infection.
876
877 Supplementary File 16. Table of enrichment results of regulatory activity in early-life adversity
878 associated CpGs relative to regulatory activity in all CpGs on the associated Illumina array.
879
880 Supplementary File 17. Library diversity of replicate transformations using the ENCODE
881 Project's PCR bottleneck coefficient (PBC).

882 **References**

883 Anders S, Pyl PT, Huber W (2014) HTSeq–A Python framework to work with high-
884 throughput sequencing data. Bioinformatics, btu638.
885 Aracena KA, Lin Y-L, Luo K, Pacis A, Gona S, Mu Z, Yotova V, Sindeaux R, Pramatarova A,
886 Simon M-M (2022) Epigenetic variation impacts ancestry-associated differences in
887 the transcriptional response to influenza infection. bioRxiv.
888 Aristizabal MJ, Anreiter I, Halldorsdottir T, Odgers CL, McDade TW, Goldenberg A,
889 Mostafavi S, Kobor MS, Binder EB, Sokolowski MB (2020) Biological embedding of
890 experience: A primer on epigenetics. Proceedings of the National Academy of
891 Sciences, **117**, 23261-23269.
892 Arnold CD, Gerlach D, Stelzer C, Boryń ŁM, Rath M, Stark A (2013) Genome-wide
893 quantitative enhancer activity maps identified by STARR-seq. Science, **339**, 1074-
894 1077.
895 Cain DW, Cidlowski JA (2017) Immune regulation by glucocorticoids. Nature Reviews
896 Immunology, **17**, 233-247.
897 Cao-Lei L, Massart R, Suderman MJ, Machnes Z, Elgbeili G, Laplante DP, Szyf M, King S
898 (2014) DNA methylation signatures triggered by prenatal maternal stress exposure
899 to a natural disaster: Project Ice Storm. PloS one, **9**, e107653.
900 Chaudhri VK, Dienger-Stambaugh K, Wu Z, Shrestha M, Singh H (2020) Charting the cis-
901 regulome of activated B cells by coupling structural and functional genomics. Nature
902 Immunology, **21**, 210-220.
903 Chen K, Liu J, Cao X (2017) Regulation of type I interferon signaling in immunity and
904 inflammation: A comprehensive review. Journal of autoimmunity, **83**, 1-11.
905 Demetriou CA, van Veldhoven K, Relton C, Stringhini S, Kyriacou K, Vineis P (2015)
906 Biological embedding of early‐life exposures and disease risk in humans: a role for
907 DNA methylation. European journal of clinical investigation, **45**, 303-332.
908 Dobin A, Davis CA, Schlesinger F, Drenkow J, Zaleski C, Jha S, Batut P, Chaisson M, Gingeras
909 TR (2013) STAR: ultrafast universal RNA-seq aligner. Bioinformatics, **29**, 15-21.
910 Dolinoy DC, Weidman JR, Waterland RA, Jirtle RL (2006) Maternal genistein alters coat
911 color and protects Avy mouse offspring from obesity by modifying the fetal
912 epigenome. Environmental health perspectives, **114**, 567-572.
913 ENCODE (2012) An integrated encyclopedia of DNA elements in the human genome.
914 Nature, **489**, 57.
915 Ernst J, Kellis M (2012) ChromHMM: automating chromatin-state discovery and
916 characterization. Nature methods, **9**, 215-216.
917 Fanucchi S, Domínguez-Andrés J, Joosten LA, Netea MG, Mhlanga MM (2021) The
918 intersection of epigenetics and metabolism in trained immunity. Immunity, **54**, 32-
919 43.
920 Gallego Romero I, Lea AJ (2022) Leveraging massively parallel reporter assays for
921 evolutionary questions. arXiv e-prints, arXiv: 2204.05857.
922 Gao T, He B, Liu S, Zhu H, Tan K, Qian J (2016) EnhancerAtlas: a resource for enhancer
923 annotation and analysis in 105 human cell/tissue types. Bioinformatics, **32**, 3543-
924 3551.
925 Greenberg MV, Bourc'his D (2019) The diverse roles of DNA methylation in mammalian
926 development and disease. Nature reviews Molecular cell biology, **20**, 590-607.

927 Harrison GF, Sanz J, Boulais J, Mina MJ, Grenier J-C, Leng Y, Dumaine A, Yotova V, Bergey
928 CM, Nsobya SL (2019) Natural selection contributed to immunological differences
929 between hunter-gatherers and agriculturalists. Nature ecology & evolution, **3**, 1253-
930 1264.
931 Heinz S, Benner C, Spann N, Bertolino E, Lin YC, Laslo P, Cheng JX, Murre C, Singh H, Glass
932 CK (2010) Simple combinations of lineage-determining transcription factors prime
933 cis-regulatory elements required for macrophage and B cell identities. Molecular
934 cell, **38**, 576-589.
935 Hertzman C (1999) The biological embedding of early experience and its effects on health
936 in adulthood. Annals of the New York Academy of Sciences, **896**, 85-95.
937 Hertzman C (2012) Putting the concept of biological embedding in historical perspective.
938 Proceedings of the National Academy of Sciences, **109**, 17160-17167.
939 Hertzman C, Boyce T (2010) How experience gets under the skin to create gradients in
940 developmental health. Annual review of public health, **31**, 329-347.
941 Husquin LT, Rotival M, Fagny M, Quach H, Zidane N, McEwen LM, MacIsaac JL, Kobor MS,
942 Aschard H, Patin E (2018) Exploring the genetic basis of human population
943 differences in DNA methylation and their causal impact on immune gene regulation.
944 Genome biology, **19**, 1-17.
945 Johnson GD, Barrera A, McDowell IC, D'Ippolito AM, Majoros WH, Vockley CM, Wang X,
946 Allen AS, Reddy TE (2018) Human genome-wide measurement of drug-responsive
947 regulatory activity. Nature communications, **9**, 1-9.
948 Kamada R, Yang W, Zhang Y, Patel MC, Yang Y, Ouda R, Dey A, Wakabayashi Y, Sakaguchi K,
949 Fujita T (2018) Interferon stimulation creates chromatin marks and establishes
950 transcriptional memory. Proceedings of the National Academy of Sciences, **115**,
951 E9162-E9171.
952 Kazachenka A, Bertozzi TM, Sjoberg-Herrera MK, Walker N, Gardner J, Gunning R, Pahita E,
953 Adams S, Adams D, Ferguson-Smith AC (2018) Identification, characterization, and
954 heritability of murine metastable epialleles: implications for non-genetic
955 inheritance. Cell, **175**, 1259-1271. e1213.
956 Killip MJ, Fodor E, Randall RE (2015) Influenza virus activation of the interferon system.
957 Virus research, **209**, 11-22.
958 Kreibich E, Kleinendorst R, Barzaghi G, Kaspar S, Krebs AR (2023) Single-molecule
959 footprinting identifies context-dependent regulation of enhancers by DNA
960 methylation. Molecular Cell.
961 Kribelbauer JF, Laptenko O, Chen S, Martini GD, Freed-Pastor WA, Prives C, Mann RS,
962 Bussemaker HJ (2017) Quantitative analysis of the DNA methylation sensitivity of
963 transcription factor complexes. Cell reports, **19**, 2383-2395.
964 Krueger F (2015) Trim Galore.
965 http://wwwbioinformaticsbabrahamacuk/projects/trim_galore/.
966 Landt SG, Marinov GK, Kundaje A, Kheradpour P, Pauli F, Batzoglou S, Bernstein BE, Bickel
967 P, Brown JB, Cayting P (2012) ChIP-seq guidelines and practices of the ENCODE and
968 modENCODE consortia. Genome research, **22**, 1813-1831.
969 Law CW, Chen Y, Shi W, Smyth GK (2014) Voom: precision weights unlock linear model
970 analysis tools for RNA-seq read counts. Genome biology, **15**, R29.

971 Lea AJ, Vockley CM, Johnston RA, Del Carpio CA, Barreiro LB, Reddy TE, Tung J (2018)
972 Genome-wide quantification of the effects of DNA methylation on human gene
973 regulation. Elife, **7**, e37513.
974 Leek JT, Johnson WE, Parker HS, Jaffe AE, Storey JD (2012) The sva package for removing
975 batch effects and other unwanted variation in high-throughput experiments.
976 Bioinformatics, **28**, 882-883.
977 Lei Y, Zhang X, Su J, Jeong M, Gundry MC, Huang Y-H, Zhou Y, Li W, Goodell MA (2017)
978 Targeted DNA methylation in vivo using an engineered dCas9-MQ1 fusion protein.
979 Nature communications, **8**, 1-10.
980 Li H, Durbin R (2009) Fast and accurate short read alignment with Burrows–Wheeler
981 transform. Bioinformatics, **25**, 1754-1760.
982 Li H, Handsaker B, Wysoker A, Fennell T, Ruan J, Homer N, Marth G, Abecasis G, Durbin R
983 (2009) The sequence alignment/map format and SAMtools. Bioinformatics, **25**,
984 2078-2079.
985 Liu PZ, Nusslock R (2018) How stress gets under the skin: early life adversity and
986 glucocorticoid receptor epigenetic regulation. Current genomics, **19**, 653-664.
987 Maeder ML, Angstman JF, Richardson ME, Linder SJ, Cascio VM, Tsai SQ, Ho QH, Sander JD,
988 Reyon D, Bernstein BE (2013) Targeted DNA demethylation and activation of
989 endogenous genes using programmable TALE-TET1 fusion proteins. Nature
990 biotechnology, **31**, 1137-1142.
991 Meissner A, Gnirke A, Bell GW, Ramsahoye B, Lander ES, Jaenisch R (2005) Reduced
992 representation bisulfite sequencing for comparative high-resolution DNA
993 methylation analysis. Nucleic acids research, **33**, 5868-5877.
994 O'Malley RC, Huang S-sC, Song L, Lewsey MG, Bartlett A, Nery JR, Galli M, Gallavotti A, Ecker
995 JR (2016) Cistrome and epicistrome features shape the regulatory DNA landscape.
996 Cell, **165**, 1280-1292.
997 Ostuni R, Piccolo V, Barozzi I, Polletti S, Termanini A, Bonifacio S, Curina A, Prosperini E,
998 Ghisletti S, Natoli G (2013) Latent enhancers activated by stimulation in
999 differentiated cells. Cell, **152**, 157-171.
1000 Pacis A, Mailhot-Léonard F, Tailleux L, Randolph HE, Yotova V, Dumaine A, Grenier J-C,
1001 Barreiro LB (2019) Gene activation precedes DNA demethylation in response to
1002 infection in human dendritic cells. Proceedings of the National Academy of Sciences,
1003 **116**, 6938-6943.
1004 Pacis A, Tailleux L, Morin AM, Lambourne J, MacIsaac JL, Yotova V, Dumaine A, Danckaert A,
1005 Luca F, Grenier J-C (2015) Bacterial infection remodels the DNA methylation
1006 landscape of human dendritic cells. Genome research, **25**, 1801-1811.
1007 Perng Y-C, Lenschow DJ (2018) ISG15 in antiviral immunity and beyond. Nature Reviews
1008 Microbiology, **16**, 423-439.
1009 Provençal N, Arloth J, Cattaneo A, Anacker C, Cattane N, Wiechmann T, Röh S, Ködel M,
1010 Klengel T, Czamara D (2020) Glucocorticoid exposure during hippocampal
1011 neurogenesis primes future stress response by inducing changes in DNA
1012 methylation. Proceedings of the National Academy of Sciences, **117**, 23280-23285.
1013 Quinlan AR, Hall IM (2010) BEDTools: a flexible suite of utilities for comparing genomic
1014 features. Bioinformatics, **26**, 841-842.

1015 Ritchie ME, Phipson B, Wu D, Hu Y, Law CW, Shi W, Smyth GK (2015) limma powers
1016 differential expression analyses for RNA-sequencing and microarray studies.
1017 Nucleic acids research, **43**, e47-e47.
1018 Robinson MD, McCarthy DJ, Smyth GK (2010) edgeR: a Bioconductor package for
1019 differential expression analysis of digital gene expression data. bioinformatics, **26**,
1020 139-140.
1021 Sardina JL, Collombet S, Tian TV, Gómez A, Di Stefano B, Berenguer C, Brumbaugh J,
1022 Stadhouders R, Segura-Morales C, Gut M (2018) Transcription factors drive Tet2-
1023 mediated enhancer demethylation to reprogram cell fate. Cell stem cell, **23**, 727-
1024 741. e729.
1025 Shlyueva D, Stampfel G, Stark A (2014) Transcriptional enhancers: from properties to
1026 genome-wide predictions. Nature Reviews Genetics, **15**, 272-286.
1027 Smyth GK (2005) Limma: linear models for microarray data. In: Bioinformatics and
1028 computational biology solutions using R and Bioconductor, pp. 397-420. Springer.
1029 Storey JD, Tibshirani R (2003) Statistical significance for genomewide studies. Proc Natl
1030 Acad Sci U S A, **100**, 9440-9445.
1031 Sun S, Barreiro LB (2020) The epigenetically-encoded memory of the innate immune
1032 system. Current opinion in immunology, **65**, 7-13.
1033 Yim YY, Teague CD, Nestler EJ (2020) In vivo locus-specific editing of the neuroepigenome.
1034 Nature Reviews Neuroscience, **21**, 471-484.
1035 Yin Y, Morgunova E, Jolma A, Kaasinen E, Sahu B, Khund-Sayeed S, Das PK, Kivioja T, Dave
1036 K, Zhong F (2017) Impact of cytosine methylation on DNA binding specificities of
1037 human transcription factors. Science, **356**, eaaj2239.
1038
1039

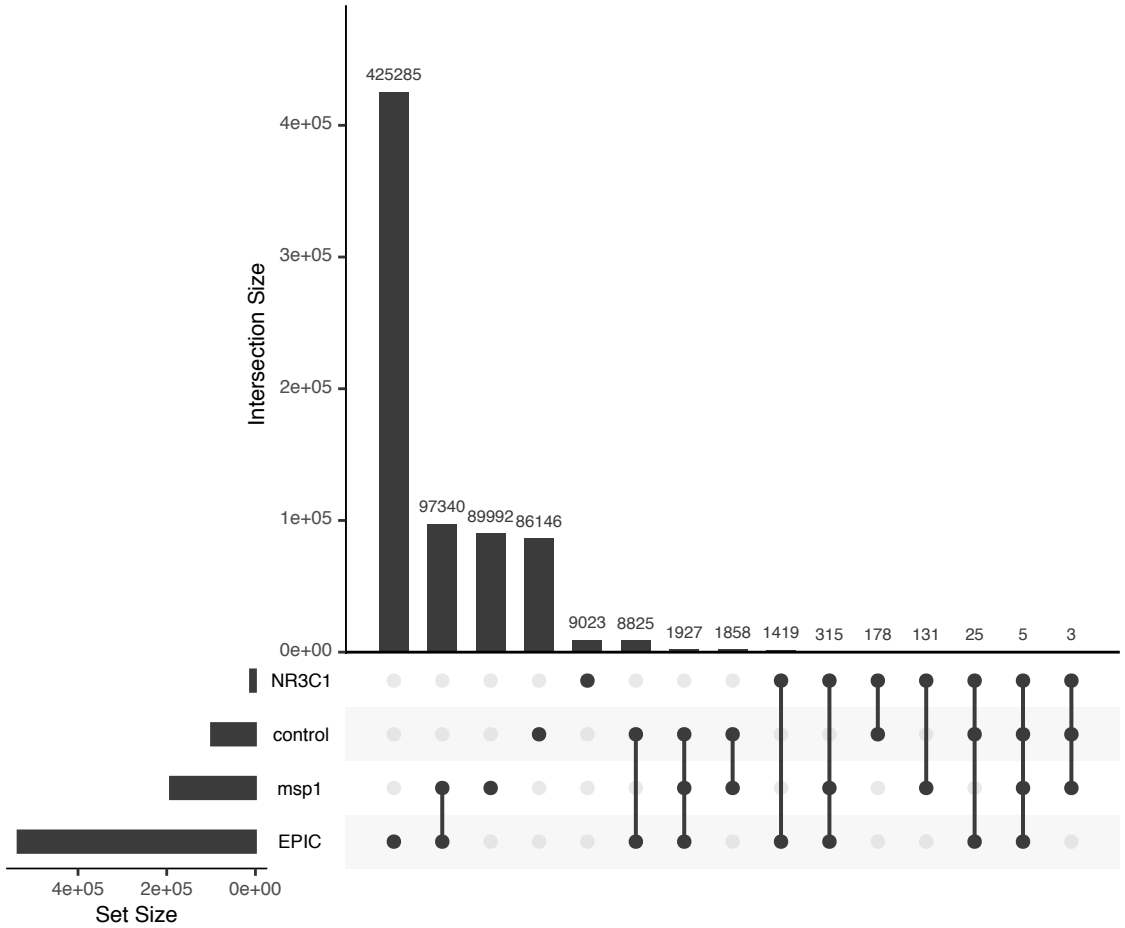

1040 **Figure 1-figure supplement 1. Overlap of target genomic regions with each other.** Upset plot
1041 showing the degree to which 600 bp non-overlapping genomic windows are shared between the
1042 four target genomic regions (EPIC CpGs, *Msp1* CpG cut sites, the *NR3C1* region, or control
1043 sites). Overlap occurs because a single 600 bp genomic window can simultaneously include
1044 EPIC CpGs, *Msp1* CpG cut sites, the *NR3C1* region, and/or control sites. This plot includes
1045 722,472 unique windows, reflecting the set of windows containing at least 1 basepair of target
1046 loci.

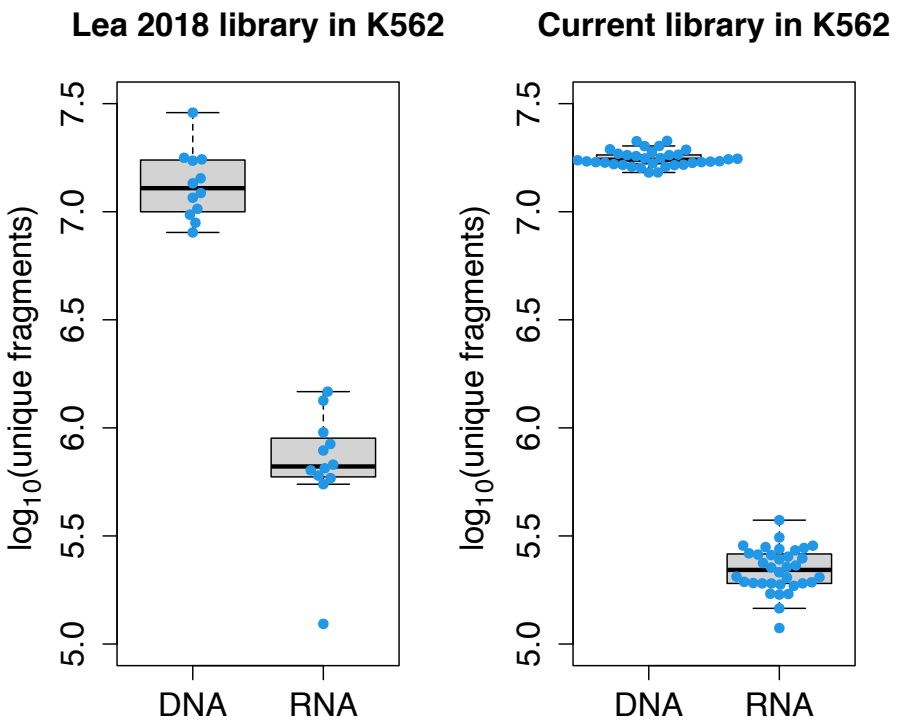

1047 **Figure 1-figure supplement 2. mSTARR-seq library diversity.** Comparison of diversity of
1048 unique mSTARR-seq DNA and RNA fragments from the library generated in this study
1049 (transfected into K562 cells) relative to the library published in Lea *et al*., 2018 (independently
1050 transfected into K562 cells). Each dot represents an experimental replicate. Each box represents
1051 the interquartile range, with the median value depicted as a horizontal bar. Whiskers extend to
1052 the most extreme values within 1.5x of the interquartile range.

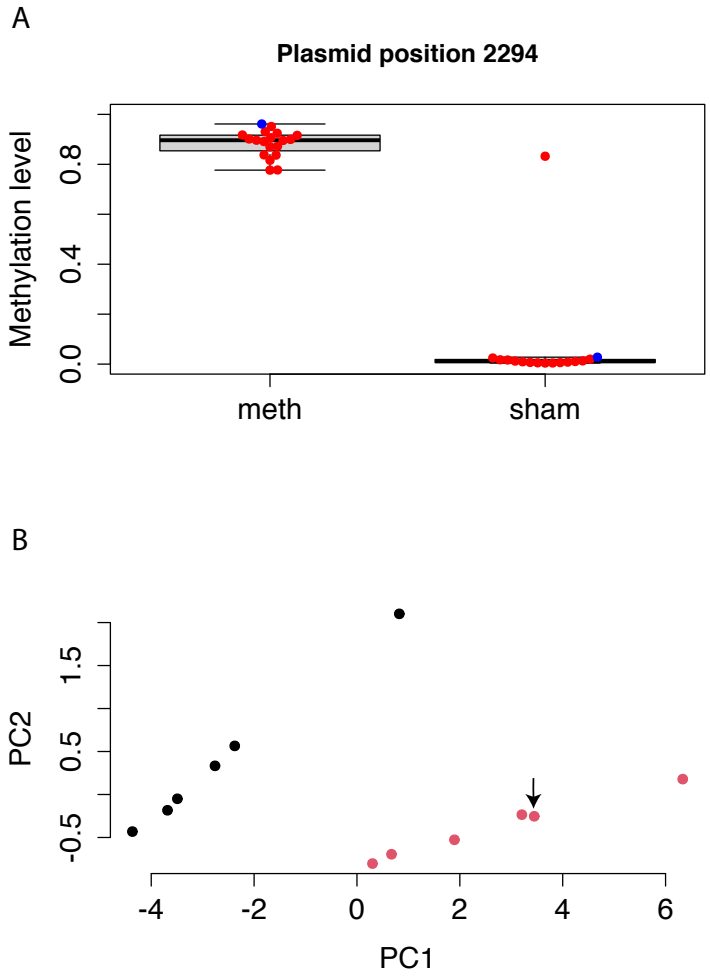

Figure 1-figure supplement 3. Methylation levels of mSTARR-seq DNA, pre- and post-transfection. (A) Bisulfite sequencing shows that DNA methylation on the mSTARR-seq plasmid is maintained until the end of the experiment (i.e., 48 hours after transfection), with significantly higher methylation levels in the replicates from the methyltransferase reaction relative to the replicates from the sham methyltransferase reaction (mean methylated = 0.885, mean unmethylated = 0.066; unpaired t-test: t = -14.66, df = 15,124, p = 2.39 x 10^{-10}). Each dot represents an experimental replicate. Red dots indicate post-transfection DNA samples; the single blue dot per condition indicates pre-transfection DNA methylation levels. Methylation is based on the CpG at the position 2294, which is located in the plasmid region used for Gibson assembly. One sample from the dex sham reaction, L31395, shows an unexpectedly high level of methylation, which appears to be due to an error during generation of the bisulfite sequencing library (e.g., mislabeled tube or poor bisulfite conversion), and not the experimental replicate of cells itself, as the mSTARR-seq RNA library (L31244) from the same replicate clusters with the unmethylated sham replicates as expected (panel B). **(B)** The first two principal components summarizing overall counts of mSTARR-seq reads for the dex-treated RNA samples (i.e., the raw readout of overall regulatory activity). Each dot represents an experimental replicate, with red and black indicating sham and methylated replicates, respectively. Overall regulatory activity of sample L31244 (indicated by arrow) clusters with the sham replicates as expected, suggesting that this replicate was indeed transfected with sham-treated mSTARR-seq DNA.

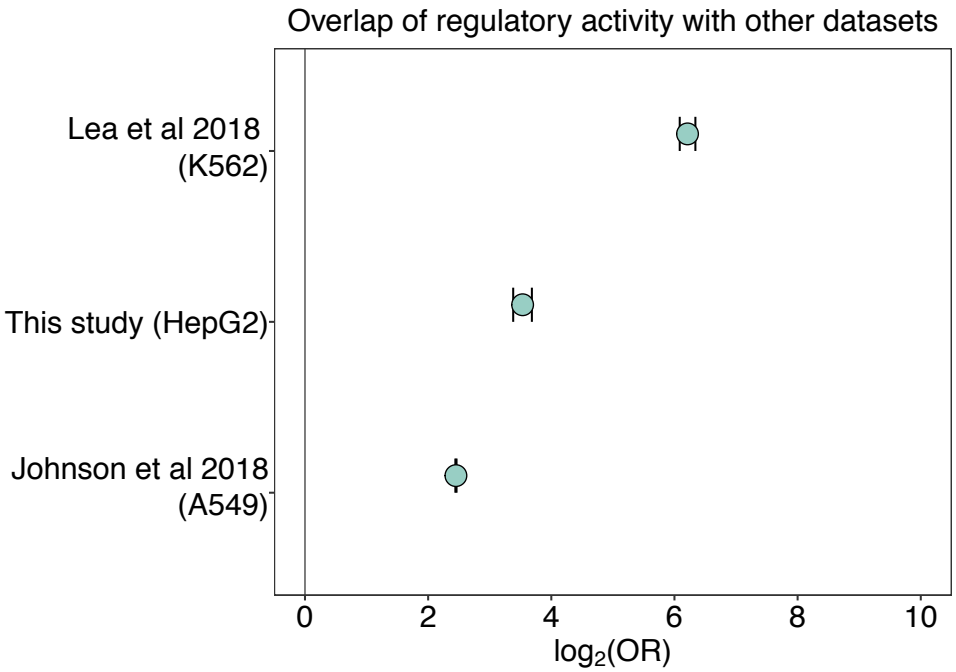

1072 **Figure 1-figure supplement 4. Overlap of regulatory activity across datasets.** Regulatory
1073 regions (in either the unmethylated sham condition, the methylated condition, or both) identified
1074 via mSTARR-seq in this study significantly overlap with: K562 regulatory regions (in either the
1075 unmethylated sham or methylated condition, or both) from a previously generated mSTARR-seq
1076 dataset reanalyzed with our pipeline (Lea et al., 2018) ($\log_2$(OR) [95% CI] = 6.212 [6.086,
1077 6.440], $p < 1.0 \times 10^{-300}$); regulatory regions (in either the unmethylated sham or methylated
1078 condition, or both) from an mSTARR-seq experiment in HepG2 liver cells ($\log_2$(OR) [95% CI] =
1079 3.534 [3.381, 3.684], $p = 5.21 \times 10^{-307}$); and regulatory regions from a conventional STARR-seq
1080 experiment (i.e., an unmethylated condition) in A549 lung epithelial cells (Johnson et al., 2018)
1081 ($\log_2$(OR) [95% CI] = 2.451 [2.442, 2.461], $p < 1.0 \times 10^{-300}$). Bars represent 95% confidence
1082 intervals.

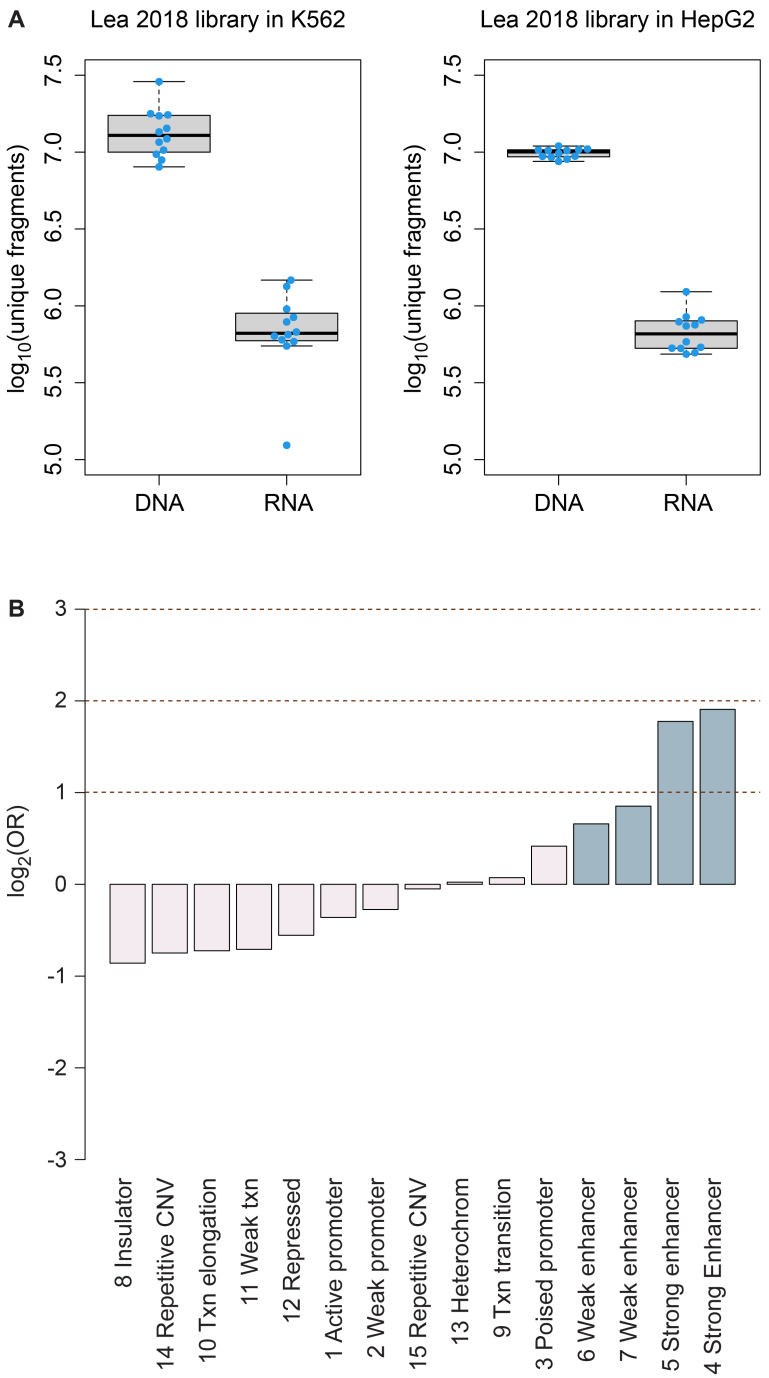

Figure 1-figure supplement 5. Library diversity and regions of regulatory activity in HepG2 cells. (A) Comparison of diversity of unique mSTARR-seq DNA and RNA fragments from the library published in Lea et al 2018 (transfected into K562 cells) versus the same library transfected into HepG2 cells in this study. Each dot represents an experimental replicate. Each box represents the interquartile range, with the median value depicted as a horizontal bar. Whiskers extend to the most extreme values within 1.5x of the interquartile range. **(B)** mSTARR-seq regulatory activity in HepG2 cells is strongly enriched in ENCODE-defined enhancers (indicated in blue) and promoters, and depleted in repressed and repetitive states.

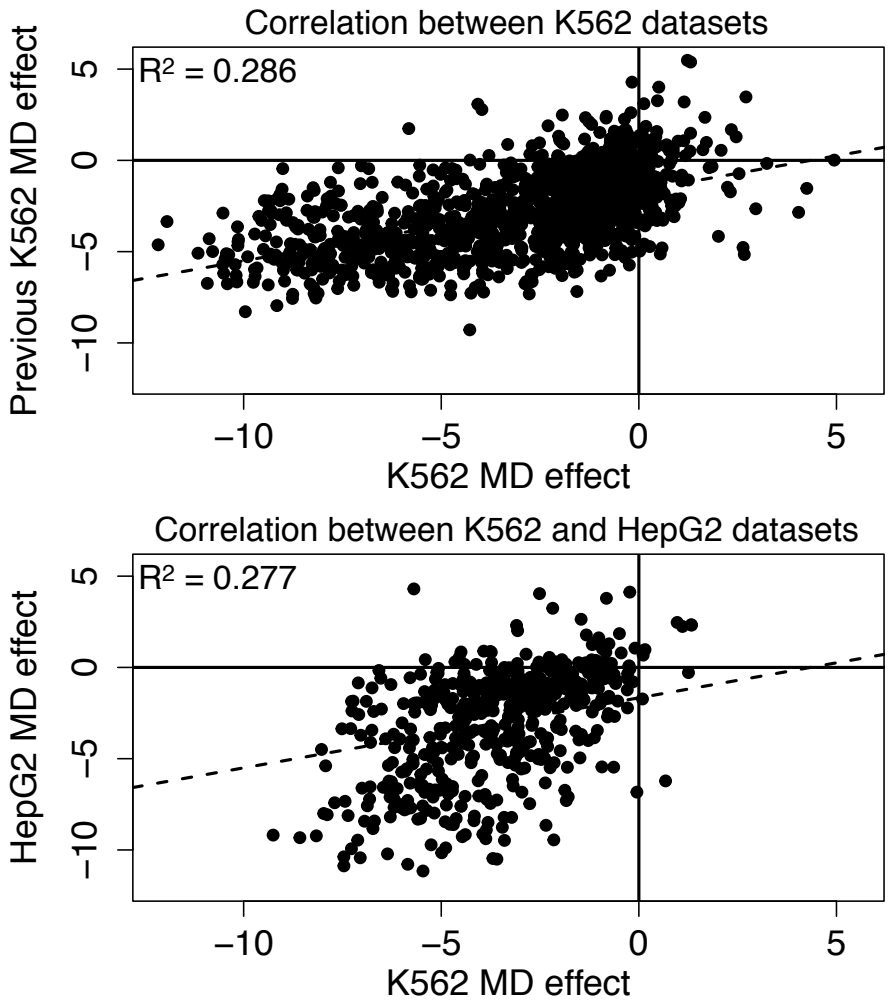

Figure 1-figure supplement 6. Methylation-dependent regulatory activity across datasets. Effects of methylation on regulatory activity estimated in this study are consistent with methylation effects in K562s estimated from a previously generated mSTARR-seq dataset (Lea et al., 2018) and with methylation effects estimated in HepG2 liver cells (K562: $R^2 = 0.286$ for 1250 windows with FDR < 1% in both data sets, $p = 3.19 \times 10^{-93}$; HepG2: $R^2 = 0.277$ for 511 windows with FDR < 1% in both data sets, $p = 8.87 \times 10^{-38}$). Each dot represents a 600 basepair regulatory window identified in both datasets (FDR < 1%; note that not all regulatory windows show significant methylation dependence (MD)). Dashed lines are the best fit lines. In all cases, negative effect sizes correspond to reduced activity in the methylated condition and positive effect sizes correspond to increased activity in the methylated condition.

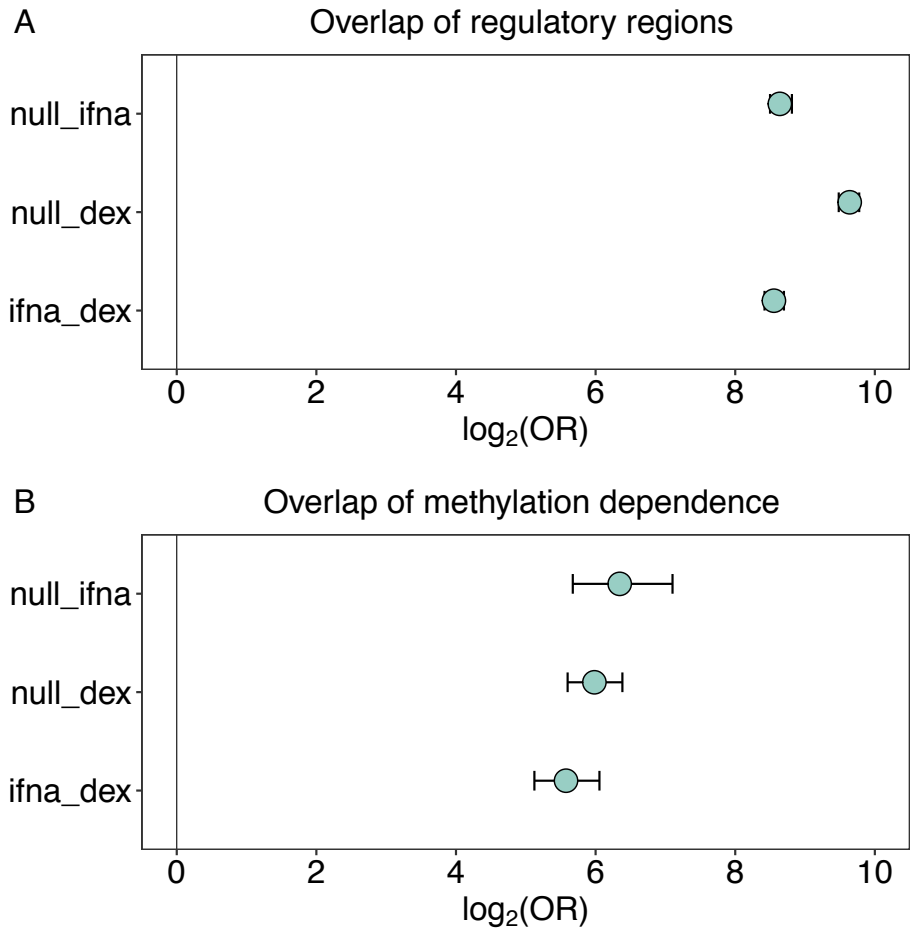

Figure 2-figure supplement 1. Regulatory activity and effects of methylation across environmental conditions. (A) Regulatory regions in the baseline condition are highly likely to retain regulatory activity upon challenge with IFNA or dex (IFNA $\log_2$(OR) [95% CI] = 8.639 [8.499, 8.812], $p < 1.0 \times 10^{-300}$; dex $\log_2$(OR) [95% CI] = 9.640 [9.483, 9.776], $p < 1.0 \times 10^{-300}$). Regulatory regions also significantly overlap between IFNA- and dex-challenged cells ($\log_2$(OR) [95% CI] = 8.554 [8.420, 8.698], $p < 1.0 \times 10^{-300}$). **(B)** Regulatory windows identified in two environmental conditions tend to share significant effects of DNA methylation on regulatory activity (i.e., interaction effects between methylation and regulatory activity) across the two environmental conditions (baseline and IFNA $\log_2$(OR) [95% CI] = 6.345 [5.673, 7.102], $p < 7.33 \times 10^{-239}$; baseline and dex $\log_2$(OR) [95% CI] = 5.982 [5.599, 6.384], $p < 1.0 \times 10^{-300}$; IFNA and dex $\log_2$(OR) [95% CI] = 5.576 [5.123, 6.055], $p < 4.70 \times 10^{-266}$).

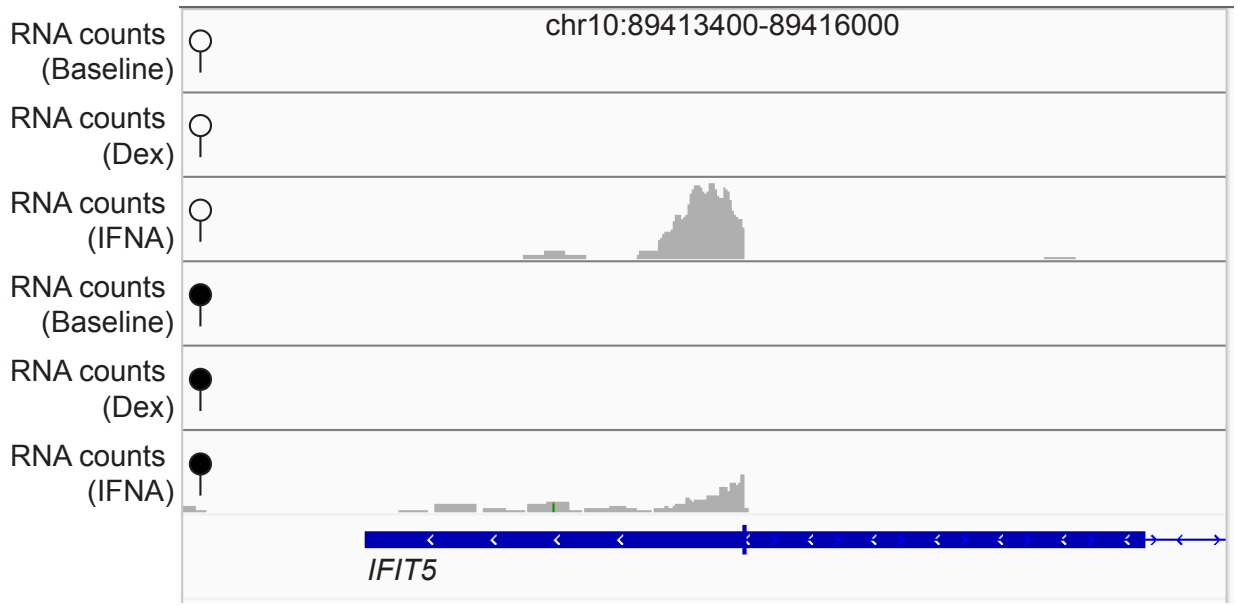

1112 **Figure 2-figure supplement 2. *IFIT5* endogenous gene expression is responsive to IFNA**
1113 **stimulation.** Tracks show non-normalized, raw read pile-ups of endogenous *IFIT5*
1114 (ENSG00000152778) gene expression in either the unmethylated (open circle) or methylated
1115 (filled circle) condition, with all y-axis maximums set to 100. The replicates for endogenous
1116 gene expression shown here are the same replicates used for measuring regulatory activity shown
1117 in Figure 2A. *IFIT5* is only detectably expressed after IFNA stimulation (note that the difference
1118 in peak heights between the IFNA-stimulated unmethylated and methylated conditions is
1119 because the plot shows raw reads; there is no effect of methylation treatment on endogenous
1120 *IFIT5* gene expression after normalization for library size: $p = 0.489$).

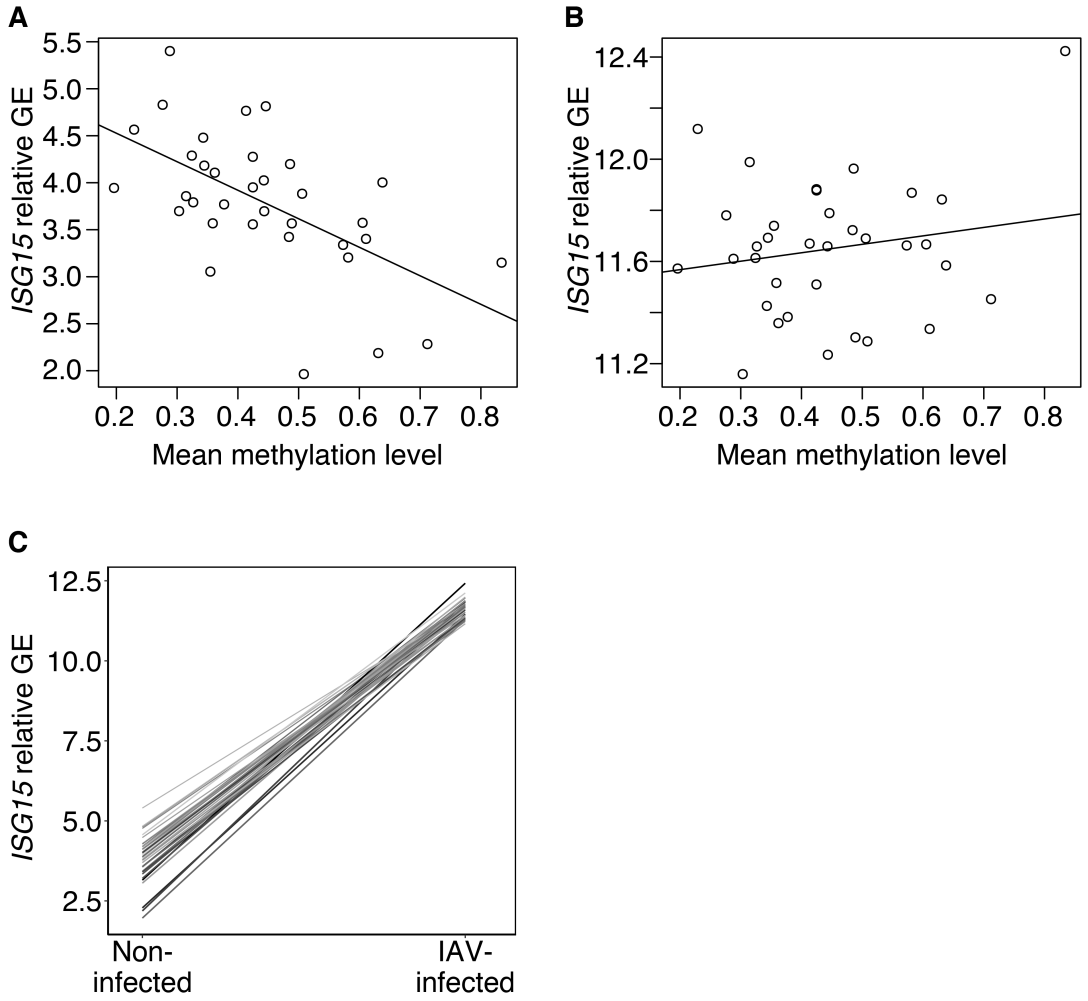

Figure 3-figure supplement 1. Across individuals, methylation in the mSTARR-seq annotated enhancer chr1:1013400-1014000 predicts the *ISG15* gene expression response to flu. (A) Across individuals, average methylation within the mSTARR-seq annotated enhancer chr1:1013400-1014000 in non-infected baseline macrophages significantly predicts *ISG15* gene expression (GE) in the non-infected condition ($R^2 = 0.324$, $p = 2.66 \times 10^{-4}$), but **(B)** not in the IAV-infected condition ($R^2 = 0.001$, $p = 0.316$). Each dot represents an individual. Relative GE is log(CPM) after regressing out the effects of sequencing batch, age, and admixture. **(C)** Individuals with relatively low methylation in the mSTARR-seq chr1:1013400-1014000 enhancer (indicated by lighter line color) in the baseline, non-infected condition tend to have higher *ISG15* gene expression in the non-infected condition, ultimately resulting in a shallower *ISG15* transcriptional response to IAV infection (as indicated by slope of the line). Each line represents an individual.

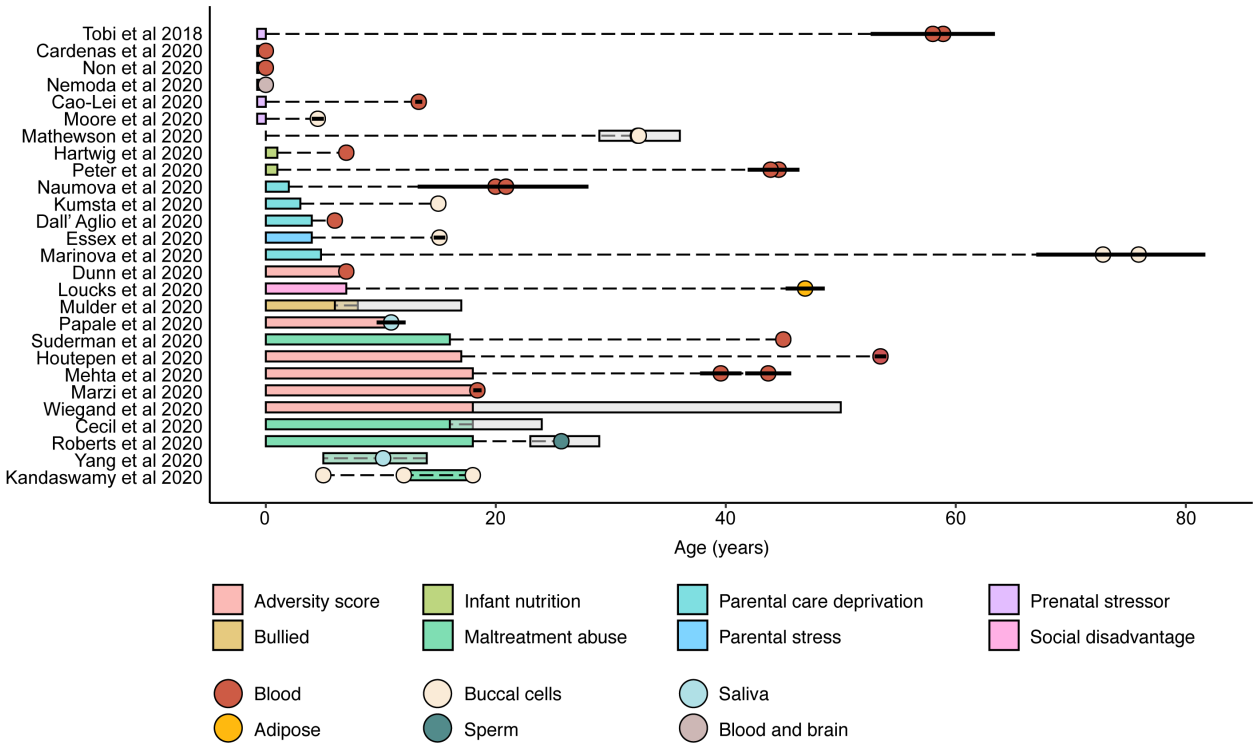

Figure 4-figure supplement 1. Summary of early-life adversity (ELA) studies. Colored and gray rectangles indicate ranges of age at adversity and at sample collection, respectively. Circles represent mean ages at sample collection and are colored according to the tissue type used to measure methylation levels. Black solid line indicates standard errors of ages at sample collection. See Supplementary File 16 for results of Fisher's exact tests assessing enrichment of ELA-associated CpGs for regulatory activity.